Geophys. J. Int. (1996) **126**, 663–688

A microseismic study in the western part of the Gulf of Corinth (Greece): implications for large-scale normal faulting mechanisms

A. Rigo,[1,*] H. Lyon-Caen,[1] R. Armijo,[1] A. Deschamps,[2] D. Hatzfeld,[3]
K. Makropoulos,[4] P. Papadimitriou[4] and I. Kassaras[4]

[1] *Équipe de Sismotectonique – CNRS URA 195 et 1093 – Institut de Physique du Globe de Paris, 4 Place Jussieu, 75252 Paris Cedex 05, France*
[2] *Institut de Géodynamique, UMR géosciences Ajur, EP125, CNRS-UNSA, 250 rue A. Einstein, 06560 Valbonne, France*
[3] *L.G.I.T-I.R.I.G.M., CNRS URA 733, Université Joseph Fourrier, BP 68, 38402 St Martin d'Hères Cedex, France*
[4] *University of Athens, Department of Geology, Geophysics-Geothermy Division, Panepistimiopolis Ilissia, Athens 157 84, Greece*

Accepted 1996 March 19. Received 1996 March 19; in original form 1995 July 17

SUMMARY

We present the results of a dense seismological experiment in the western part of the Gulf of Corinth (Psathopyrgos–Aigion area), one of the most active rifts in the Aegean region for which we have precise tectonic information. The network included 51 digital stations that operated during July and August 1991, covering a surface of 40×40 km^2. Among the 5000 recorded events with M_L ranging between 1.0 and 3.0, we precisely located 774 events. We obtained 148 well-constrained focal mechanisms using *P*-wave first motions. Of these, 60 also have mechanisms obtained by combining the *P*-wave first motions with the *S*-wave polarization directions. The observed seismicity is mainly located between 6 and 11 km depth. Most of the fault-plane solutions correspond to E–W-striking normal faulting, in agreement with the geological evidence. Most of the well-determined mechanisms indicate a nodal plane dipping 10–25° due north and a steep south-dipping plane. A similar asymmetry is also seen in the seismicity distribution and in the overall geological structure of the Corinth Rift. We discuss this evidence and the inference of a deep detachment zone, a structure where the major faults seen at the surface appear to root. A large part of the microseismic activity appears to cluster in regions near the junctions of the main faults with the proposed detachment zone. This feature of the microseismicity is interpreted in terms of stress transfer and stress concentration in regions of probable nucleation of future large earthquakes.

Key words: fault-plane solutions, Greece, Gulf of Corinth, normal faulting, microseismicity.

1 INTRODUCTION

One important problem in seismotectonics is to characterize the loading process on large active fault systems and to understand the temporal and spatial relationships between small-scale faulting, microseismicity and large destructive earthquakes. How strains accommodate near the base of the seismogenic layer where large earthquakes nucleate is of particular interest in understanding the mechanisms by which stresses build up. In the case of crustal extension, it is commonly accepted that the normal faults capable of generating large earthquakes usually cut the entire seismogenic layer, but how these faults root into the deeper semi-brittle and ductile layers remains largely unknown. An asymmetric deep structure is often inferred from seismic profiles for continental areas under extension (Covington 1983; Arabasz & Julander 1986; Logatchev & Zorin 1987; Maier & Eisbacher 1991; Wenzel *et al.* 1991). This implies the existence of crustal detachments or large shear zones dipping less than 30°. Studies of large continental normal-faulting earthquakes, however, show that they generally initiate in the upper brittle crust and the fault-plane solutions do not exhibit low-angle nodal planes (e.g. Jackson & White 1989), with the possible exception of the Woodlark–D'Entrecasteaux earthquake (Abers 1991). In some large earthquakes, secondary rupture on low-angle normal faults has also been suggested (e.g. Eyidogan & Jackson 1985; Bernard & Zollo 1989a). However, the study of the deeper parts of the faults is hampered by the insufficiency of well-defined seismicity.

* Now at: Observatoire Midi-Pyrénées–GRGS–CNRS UMR 5562, 14 Ave. E. Belin, 31400 Toulouse, France.

One possible way to define the fault geometry at depth is to study the deformation in the semi-brittle transition zone by means of its microseismic activity. This can be criticized because fault-plane solutions of microearthquakes do not usually show a simple pattern (e.g. Jackson & White 1989). The main difficulties with this method are (1) to appraise the relationship of the observed microseismic activity (recorded during short periods of time) with the seismic cycle, and (2) to ascribe this activity to the major faults or to the network of fractures surrounding them. A way to overcome these problems is to install very dense networks of portable seismological stations in rapidly deforming areas with high seismicity. However, previous experiments in Greece (Melis *et al.* 1989; Hatzfeld *et al.* 1990) and in the Basin and Range (Jones 1987) had no conclusive results about the normal-faulting geometry at depth, possibly because the deployed networks were not dense enough.

The Gulf of Corinth is one of the most prominent active rifts in the Aegean area, with a history of repeated large earthquakes and with a high level of background seismicity (Papazachos & Papazachos 1989; Ambraseys & Jackson 1990). Large earthquakes occurred in 1861 near the city of Aigion ($M_w = 6.7$) (Papazachos & Papazachos 1989), producing 13 km long surface breaks (Schmidt 1881), and in 1981 near Corinth, with a sequence of three events ($M_s = 6.7$, 6.4, 6.4) (Jackson *et al.* 1982; King, Oppenheimer & Amelung 1985) (Fig. 1). The geological evidence suggests an unusually fast Quaternary slip rate of the order of 1 cm yr^{-1} on the major E–W-striking, north-dipping normal faults at the southern edge of the Corinth rift, which appears to be mostly an asymmetric structure (Armijo *et al.* 1996).

In 1991, we began a multidisciplinary study, which included the tectonics, the geodesy and the microseismicity of the Gulf of Corinth. Detailed accounts of the tectonic results are given elsewhere (Armijo *et al.* 1996), and a synoptic view of the overall work can be found in Rigo (1994). Here, we present the main results of an experiment in July and August 1991 with a dense network of digital seismological stations installed in the western part of the Gulf. The experiment was designed to cover, at the appropriate scale and with reasonably good hypocentral resolution, an area where the near-surface geometry of the main faults was well constrained. Previous background seismicity proved to be high in the region between the cities of Patras, Aigion and Navpaktos (Galanopoulos 1960, 1961; Melis *et al.* 1989; Hatzfeld *et al.* 1990; Amorese 1993). During our six week experiment we recorded a total of about 5000 events, providing us with a consistent data set from which we obtained accurate earthquake locations and well-constrained fault-plane solutions. We use this data together with the tectonic observations to bring constraints on the geometry of the faults and on the mechanism of normal faulting at depth.

2 SEISMOLOGICAL DATA ANALYSIS

2.1 Network and locations

The seismological network, composed of 51 digital portable stations (Fig. 2; Appendix A), covered an area about

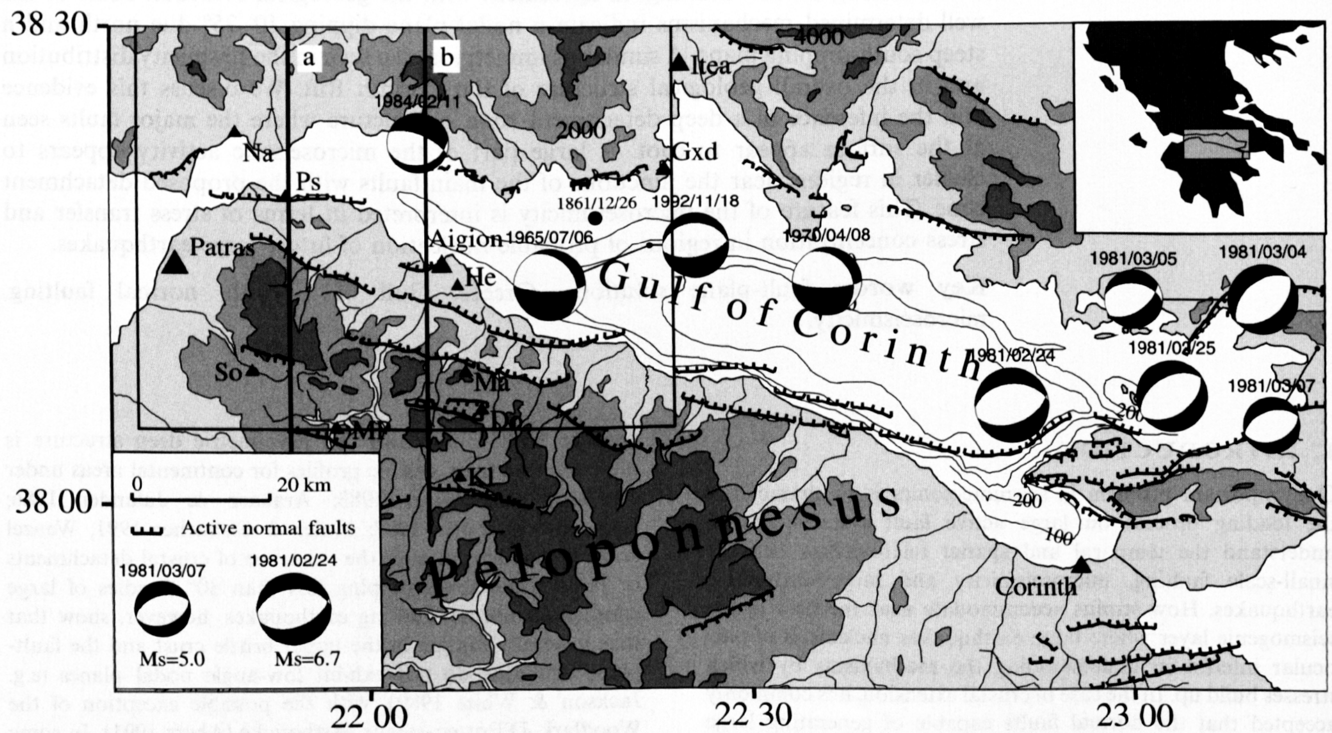

Figure 1. Seismotectonic map of the Gulf of Corinth. Active faults are mapped from field observations and SPOT images (Armijo *et al.* 1996). Elevation contours are in feet. Fault-plane solutions of 1965–92 events with magnitude larger than 5 are from Ambraseys & Jackson (1990), Taymaz, Jackson & McKenzie (1991) and Briole *et al.* (1993). The epicentre of the 1861/12/26 earthquake (black dot) is from Schmidt (1881). a and b indicate locations of sections in Fig. 12. Do: Doumena; Gxd: Galaxidi; He: Helike; Kl: Kalavrita; Ma: Mamousia; MP: Megas Pontias; Na: Navpaktos; Ps: Psathopyrgos; So: Souli. The inset outlines the area studied (Figs 2 and 8).

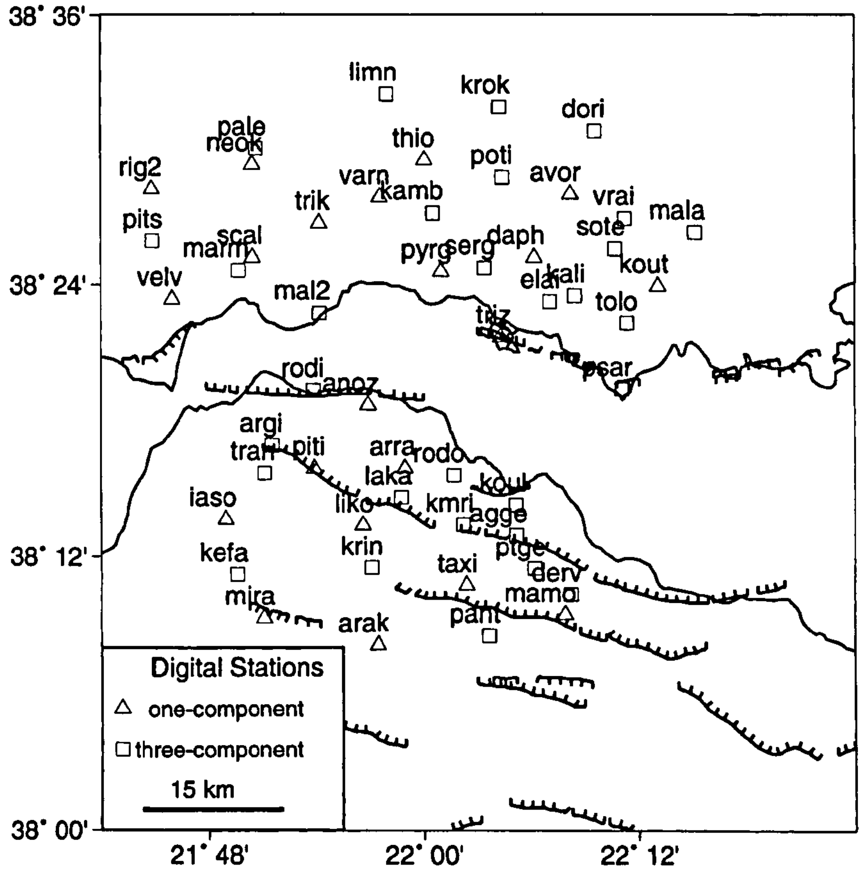

Figure 2. Network in operation from 10/07/1991–26/08/1991. Coordinates of the stations are given in Appendix A.

40 km × 40 km, with an average distance between stations of 3–6 km. The stations were equipped with 1 or 2 Hz seismometers. The 21 one-component stations had a recording frequency of 100 Hz; for the three-component stations, 15 had a recording frequency of 125 Hz, 12 had one of 200 Hz, and 3 had one of 62.5 Hz. Absolute time was given by the DCF time code recorded in parallel with the internal station clock for all three-component stations. For the one-component stations, the internal clock was permanently reset on the DCF time code. Thus the time accuracy is estimated to be better or of the order of the sampling rate. The time-reading precision is estimated to be between 0.005 and 0.06 s for *P* waves, and between 0.01 and 0.1 s for *S* waves, depending on the recording system.

About 5000 events with magnitude M_L between 1 and 3.0 were recorded during the six weeks of the experiment. Here, we analyse a subset of 850 events recorded by at least five stations during the month of August when the network was completely installed. The hypocentral locations were computed using the HYPO71 code (Lee & Lahr 1975). As no crustal velocity structure is available for the area, we constructed a mean velocity model from our data set. We estimated the V_p/V_s ratio to be 1.80 ± 0.02 from Wadati diagrams constructed using the three-component records only. This ratio is in agreement with the values ranging between 1.77 and 1.83 obtained in the neighbouring areas (e.g. King *et al.* 1985; Melis *et al.* 1989; Hatzfeld *et al.* 1990; Amorese 1993). We first determined the mean *P* velocity between 0 and 15 km depth by studying the variation of the mean rms traveltime residual with respect to this mean velocity (Fig. 3). The mean rms is minimum between 5.4 and 5.7 km s^{-1}. Then, taking a velocity of 5.7 km s^{-1} as a reference, we computed the number of events for which the rms decreases when using a different velocity. For a value of 5.6 km s^{-1}, 90 per cent of the events have their rms reduced. A similar result was obtained with other reference velocities. We thus used a 5.6 km s^{-1} mean *P* velocity between 0 and 15 km (model 1—Table 1). Comparable mean velocities were found in the area (e.g. King *et al.* 1985; Melis *et al.* 1989; Amorese 1993). Our data provide no information on the velocity below 15 km depth because of the lack of events at these depths. We thus fixed the velocities there as in the previous studies mentioned above (Table 1). We determined a

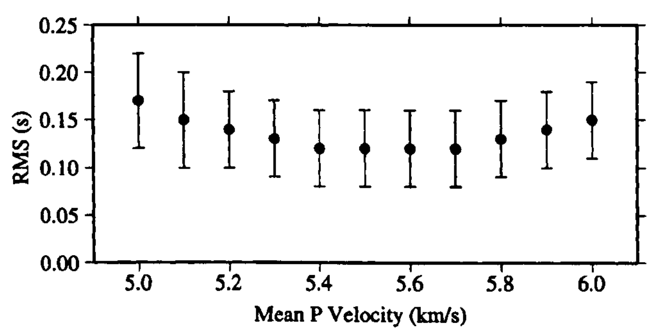

Figure 3. Mean location rms for the 850 selected events versus assumed mean *P*-wave velocities between 0 and 15 km depth. Error bars represent standard deviation.

Table 1. *P*-wave velocity models used for the earthquake locations. $V_p/V_s = 1.80$.

	Model 1	Model 2
Depth (km)	Vp (km/s)	Vp (km/s)
0.0 - 4.0		4.8
4.0 - 7.2		5.2
7.2 - 8.2	5.6	5.8
8.2 - 10.4		6.1
10.4 - 15.0		6.3
15.0 - 30.0	6.5	6.5
> 30.0	7.0	7.0

multilayer model (model 2—Table 1), keeping the 5.6 km s^{-1} mean *P* velocity in the upper 15 km, which appears to be the most appropriate for fault-plane solutions (see detailed discussion in Section 2.2). This model was then used to determine both the event locations and the fault-plane solutions.

Owing to the geometry and the density of the network, event locations are very well constrained. We performed two tests to assess the precision of focal depths. First, we compared results obtained using *initial* depths of 5 and 20 km with HYPO71. Second, we compared results obtained with velocity models 1 and 2. We rejected events for which the focal depth varied by more than 2 km to select a final set of 774 events with a precision of about ± 2 km for focal depths and ± 1 km for the epicentral positions (Appendix B). The final mean rms traveltime residual for this final set of events is 0.11 ± 0.04 s.

2.2 Fault-plane solutions

The fault-plane solutions were determined in two steps. First they were constructed by hand using only the *P* first motions. Then, when it was possible, they were better constrained using *S*-wave polarization directions, following the method developed by Zollo & Bernard (1991). In order to guarantee the quality of the determinations, we selected events with at least 10 clear *P* polarities. This restriction gave us a set of 190 events.

Velocity model 1 did not yield fault-plane solutions for many of these events because the ray's angle of incidence was too small, making it impossible to draw two perpendicular nodal planes. (See, for example, events 398 and 50 in Fig. 4.) The multilayer velocity model 2 was constructed to determine fault-plane solutions for a maximum number of events. As a first step, we proceeded by trial and error, using the 190 selected events, to introduce layers between 0 and 15 km in order to transform some direct rays into refracted rays (e.g. event 50, Fig. 4) which are clearly observed on the records. In the resulting model, the depths of the velocity interfaces are mainly constrained by the depth of the events. Clearly model 2 does not correspond to a unique solution, but it is the best layered model that we could find to reduce polarity inconsistencies in the fault-plane solutions. Tests were performed to assess the stability of the fault-plane solutions with respect to the velocities in the layers and the position of the interfaces. Because of the high density of stations in the network, fault-plane solutions are more sensitive to the location of interfaces than to the velocities in each layer. The 3-D smoothly varying velocity model obtained by tomographic inversion with the same set of data (Le Meur 1994) is consistent with model 2. The interfaces of model 2 correspond to the higher gradients of Le Meur's model. Additionally, focal mechanisms determined with model 1 did not significantly change with model 2 (e.g. event

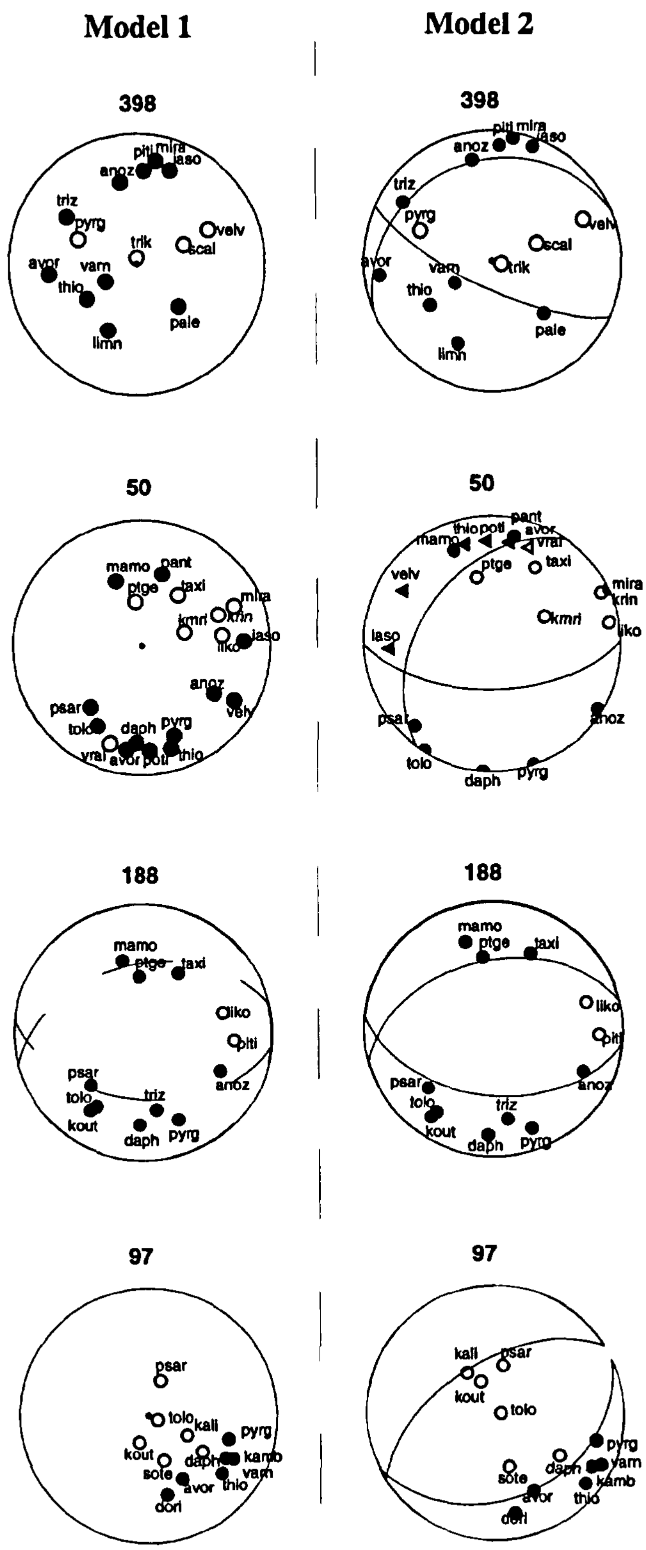

Figure 4. Focal mechanisms of four events (Appendix B) with two different velocity models (models 1 and 2, Table 1). *P* polarities are plotted on the lower equal-area hemisphere of the focal sphere. Dots represent direct rays, triangles refracted rays. Fault planes are drawn when possible. Note that in model 2 the incidence angles are increased and refracted rays are present.

188, Fig. 4). Finally, we obtained a total of 148 focal mechanisms, of which about 30 are not well constrained (e.g. event 97 in Fig. 4).

As a second step to constrain fault-plane solutions better, we combined *P*-wave polarities with *S*-wave horizontal polarization directions to estimate the fault-plane parameters (Zollo & Bernard 1991; de Chabalier *et al.* 1992). For such a study, the *S*-wave polarization must be stable in time and linear. This implies the use of incidence angles smaller than 45°. For larger incidences, free-surface effects can be important, inducing the instability of *S*-wave polarization (Evans 1984; Booth & Crampin 1985; Bernard & Zollo 1989b). To obtain more stable polarizations, the records were bandpass-filtered between 1 and 3 Hz with a zero-phase-shift Butterworth filter. However, few stations show very clear splitting of *S* waves due to crustal anisotropy (Bouin, Téllez & Bernard 1996) with time delays larger than 0.05 s between the slow and the rapid *S* arrivals. These data were not used in the inversion. Then, each selected three-component record was examined for *S*-polarization stability. In Fig. 5 we present an example of the determination of the *S*-wave polarization direction at station krin for event 447. The initial record (Fig. 5a) is filtered between 1 and 3 Hz (Fig. 5b). We represent the 3-D particle movement vector at a constant time interval on a horizontal stereographic projection for a short temporal window (1 s) for the *P* wave and the *S* wave. We can thus check that the *P*-wave incidence is vertical. If the *S*-wave polarization is stable and linear with time, the points cluster (each point representing the particle vector at a given time on the stereographic projection) around the direction of the *S*-wave polarization (west in the example of Fig. 5). The average values of the azimuths and incidence angles of the particle movement vector at the surface define the *S*-wave mean polarization direction and incidence angle. The nearer to the horizontal the *S* incidence angle is, the better the datum. The accuracy of the polarization direction depends on the size of the particle movement vector cluster, i.e. on the stability of the *S*-wave polarization with time. This accuracy is globally estimated to be 10–15°. Thus, for 60 events out of the 190 selected earlier, we were able to add information by including the *S*-wave polarization directions.

We then performed the inversion for each mechanism by searching for the best fault-plane solution corresponding to the observed *P* polarities and *S*-wave polarization directions. Because of the non-linearity of the problem, the inversion is a systematic exploration of the fault-plane parameter space (strike, dip, slip) to find the maximum of a probability density function (Brillinger, Udias & Bolt 1980; Zollo & Bernard 1991). The result of the joint inversion of *P* polarities and *S*-polarization directions for event 491 is shown in Fig. 6. The probability density function is represented by the 66, 90 and 99 per cent levels on the entire fault-plane parameter space. The clusters represent the conjugate fault planes (P1 and P2 in Fig. 6). The estimated values for strike, dip and slip are given by the position of the maximum of the density function for each nodal plane. In the example of Fig. 6, the values are: strike = 211.0°, dip = 70.0° and slip = −150.4°. The uncertainties on these values can be estimated from the area with 66 per cent probability. For a given slip and dip, the uncertainty on the strike is close to 30°; for a given strike, the uncertainties on slip and dip range between 10° and 30°. Because we have to consider the three fault-plane parameters together, the overall uncertainty of each of these parameters is about ±15°.

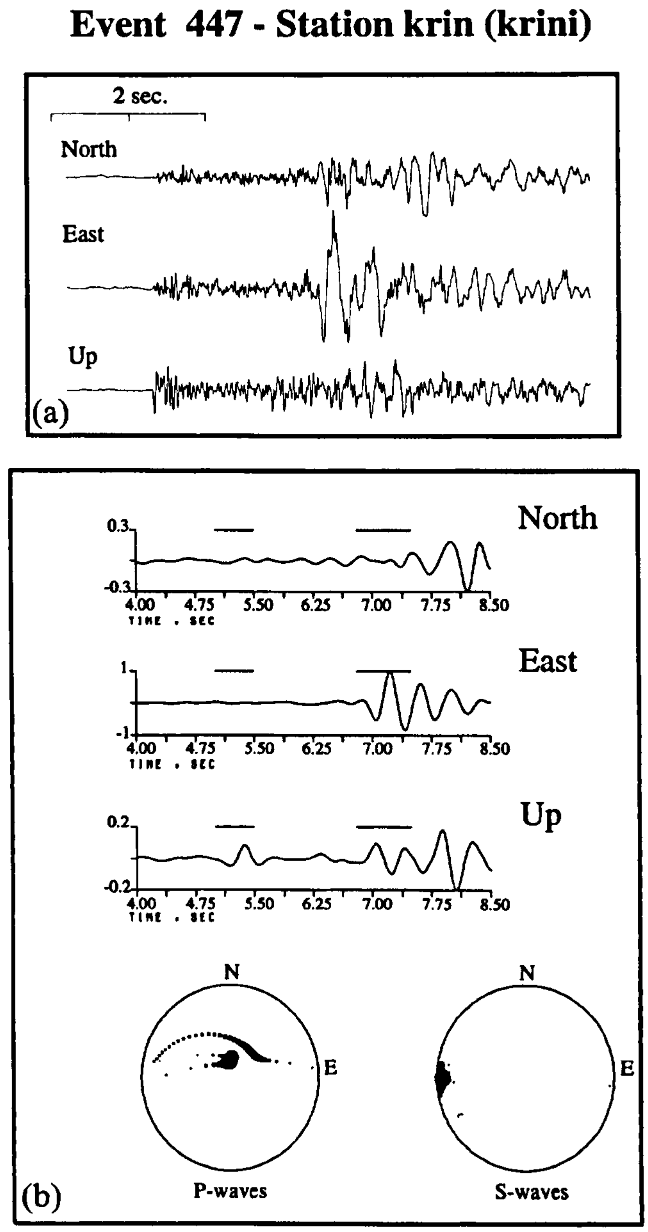

Figure 5. Example of determination of shear-wave direction of polarization. (a) Initial three-component record. (b) Same record filtered between 1 and 3 Hz (top), with particle movement vector on horizontal stereographic projection for *P* waves (bottom-left) and *S* waves (bottom-right). The time window used for *P* and *S* waves is indicated on the filtered records by horizontal lines. The direction and the dip of the *S*-wave polarization obtained here are 90.0° and 7.5° (± 3.4°), respectively.

The four examples in Fig. 7 illustrate the improvement brought by our method. We compare here the mechanisms obtained with the *P* first motions only and the mechanisms from the joint inversion of *P* polarities and *S*-polarization directions. In general, the addition of *S*-polarization directions constrains the mechanisms better. In a few cases, however (e.g. event 447, Fig. 5), the fit of *S*-polarization directions may be slightly worse for the inversion solution than the one obtained

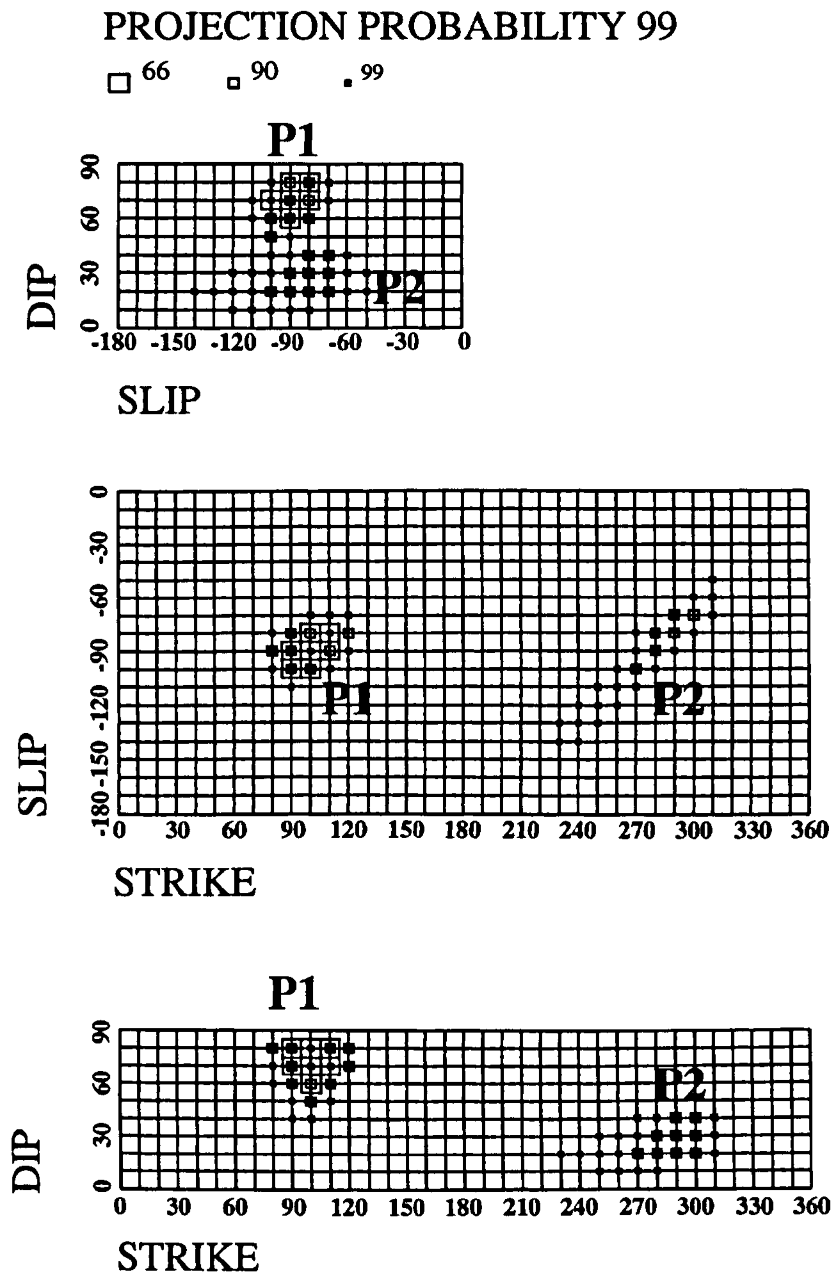

Figure 6. Result of the joint inversion of *P* polarities and *S*-wave polarization directions for event 491. Representation of the probability density function in the fault-plane parameter space (strike, dip, slip). The 66, 90 and 99 per cent confidence levels are represented with decreasing symbol sizes. The clusters correspond to the two conjugate fault planes P1 and P2.

by hand. This is related to the shape of the conditional probability density function used in the inversion. Because this function has a finite width around nodal planes, the algorithm naturally tends to favour solutions in which no station is very close to a nodal plane. In any case, variations in strike and dip between the two methods are small and within the uncertainties when both kinds of data (*P* and *S*) are well explained. In other cases, such as event 475, the mechanism, which was not well constrained in the manual solution, changes to a N–S- rather than a NW–SE-trending normal fault. Finally, events 92 and 97 (Fig. 5), which were badly constrained by the *P* polarities alone, are now better resolved.

We determined 148 focal mechanisms (Appendices C and D). In the interpretation, we always choose the solution from the joint inversion, if it exits.

3 EARTHQUAKE AND FOCAL MECHANISM DISTRIBUTION

The seismicity appears to be located beneath the Gulf and a few kilometres inland on both sides of the Gulf (Fig. 8). More activity is observed on the northern side. In addition to some distributed background seismicity, three main clusters are identified: the cluster near the city of Aigion (Cl1), which was very active during the 2 months of the experiment and should be associated with the $M_L=4.5$ event that occurred there on

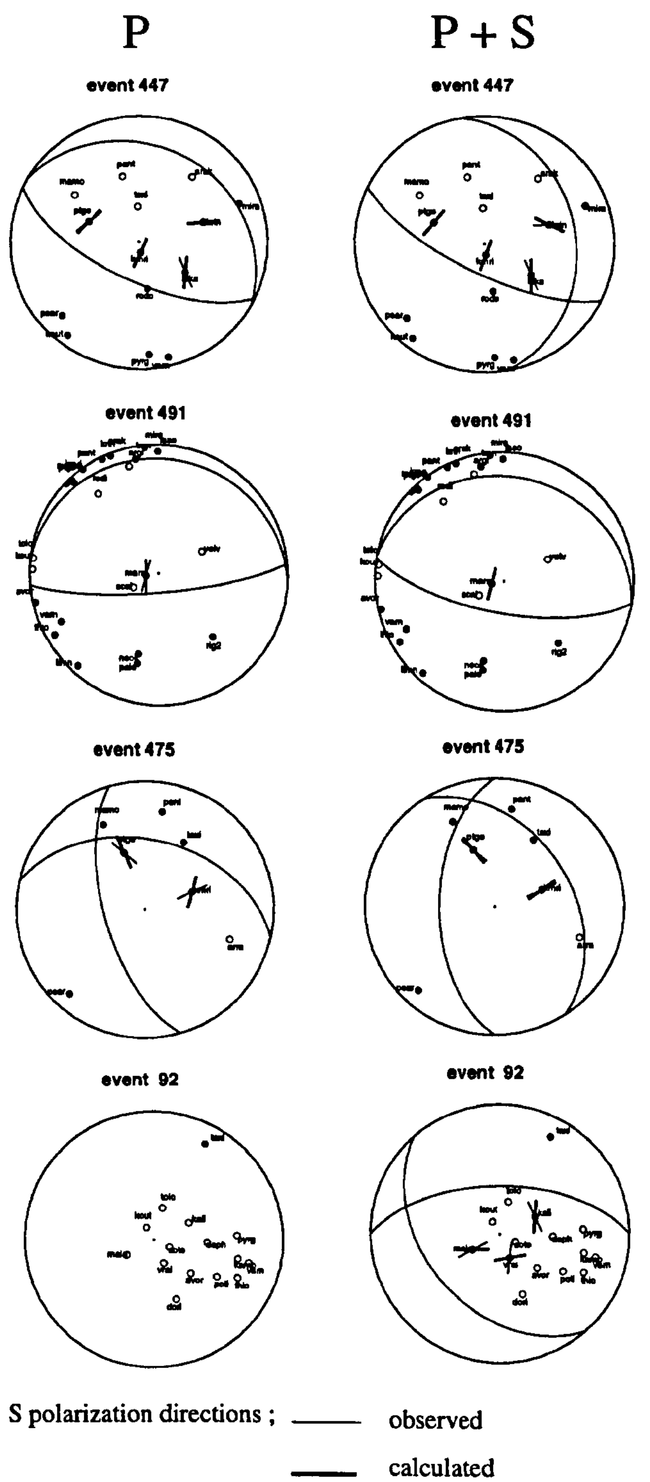

Figure 7. Comparison between focal mechanisms determined with *P* polarities only (left) and the focal mechanisms determined by joint inversion of *P* polarities and *S*-wave polarization directions (right). Thick lines are observed shear-wave polarizations and thin lines are calculated ones.

July 3; cluster Cl2, active during the month of August, with two M_L=2.8–3.0 events (47 and 677); and the cluster of August 24 (Cl3) with magnitude 2.0–2.8 events. The largest recorded events, both of magnitude M_L = 3.0, are the August 5 event (156 in Appendix B) and the August 23 event (677 in Appendix B).

The depth distribution of the events (Fig. 9) indicates that the maximum of activity is concentrated at 6–10 km depth. Moreover, 98 per cent of the events have focal depths less than 13–14 km. We deduce that the thickness of the seismogenic layer in the Patras–Aigion area does not exceed 15 km, considering the focal depth uncertainties of ± 2 km. This is in agreement with the aftershock study of the 1981 Corinth earthquakes by King *et al.* (1985), who found fewer than five events deeper than 15 km in the Corinth–Perachora region among a set of 133 well-located events. Another aspect of this vertical distribution is the absence of events shallower than 4 km (Fig. 9). We checked that this was not an artefact of our selection criteria for events. This small shallow activity is probably related to the rheological property of the shallow crustal layers, as suggested by King *et al.* (1994) for the San Andreas fault zone.

The distribution of the seismicity does not outline the geometry of the active faults at depth (Fig. 10). In the western part of the network (a1 and a2 in Fig. 10), the events align along an apparent geometry dipping 10°–20° north between 7 and 12 km depth, including cluster Cl2. This geometry does not appear clearly in the eastern sections (b and c in Fig. 10), except if we consider that it is outlined by the lower limit of the seismicity. Nevertheless, clusters Cl2 and Cl3 are in the down-dip extension of the Psathopyrgos fault (P in Fig. 10) and the Aigion fault (Ai in Fig. 10), respectively.

The fault-plane solutions yield a consistent N–S direction of extension, in agreement with the large-scale tectonics of this area (Fig. 11). The majority of the mechanisms correspond to E–W-trending normal faulting consistent with the strike of the active faults. Few strike-slip and reverse fault-plane solutions are observed (e.g. 8, 86, 294, 308, and 358 in Appendix C).

Normal-faulting mechanisms with T axes oriented N–S and nodal planes dipping north or south between 35° and 70° are found in the eastern part of the network (Fig. 11a). The mean T axes for clusters Cl1 and Cl3 are subhorizontal in both cases (Table 2).

Normal-faulting mechanisms with a N–S-oriented T axis plunging approximately 30° are found in the western part of the network (Fig. 11b). They represent normal faulting with an E–W nodal plane dipping 75°–85° south and the other nodal plane dipping 10°–25° north. Most of these mechanisms are well constrained by *S*-wave polarization directions. These peculiar fault-plane solutions are found in cluster Cl2 but also south and northwest of it.

4 DISCUSSION

To assess the significance of microearthquakes within a volume of crustal rocks with major active faults is a difficult problem.

Table 2. Mean P and T axes for each cluster deduced from fault-plane solutions. Uncertainties are 10° for the strike and 5° for the plunge.

Cluster	Mean P Axis		Mean T Axis	
	Strike (°)	Plunge (°)	Strike (°)	Plunge (°)
Cl1	103.4	78.8	184.9	13.0
Cl2	354.9	66.0	187.5	29.8
Cl3	179.7	70.8	341.4	23.8

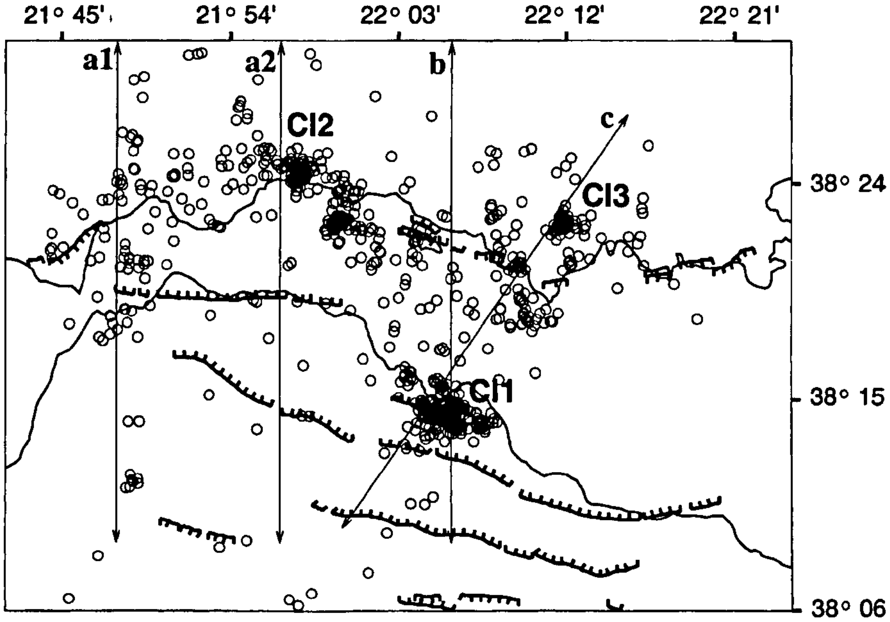

Figure 8. Locations of the 774 selected events. Segments a1, a2, b and c correspond to the sections shown in Fig. 11. Cl1, Cl2 and Cl3 indicate the three main clusters.

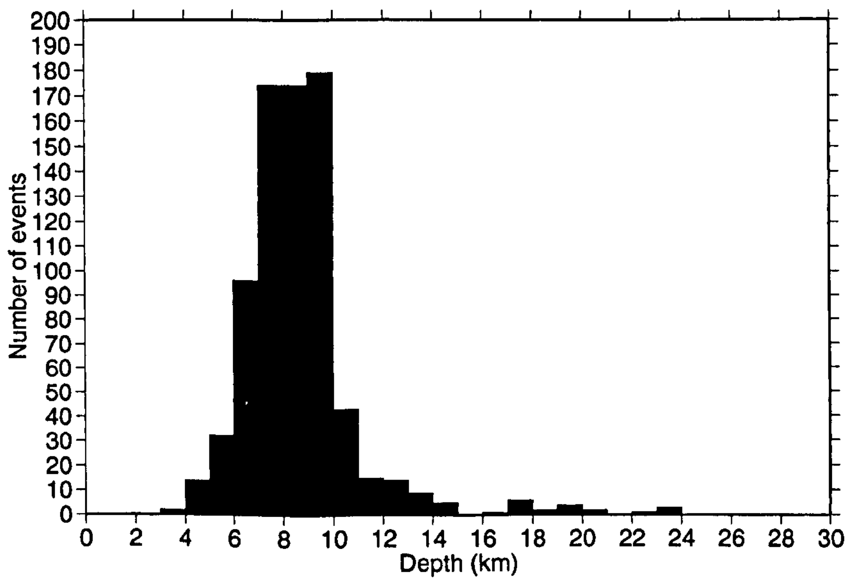

Figure 9. Vertical distribution of the 774 selected events. Uncertainties on focal depths are ±2 km. 80 per cent of the activity is located between 6 and 10 km depth.

An event of magnitude smaller than 3 is not necessarily associated with slip on a major fault. Such an event corresponds to a source radius smaller than 300–400 m with only a few millimetres of slip. Thus, microearthquakes may be associated with major fault planes but also with minor faults. The presence of fractures or fracture zones in the upper crust is commonly assumed in active tectonic regions, where they are often observed near fault planes (Chester & Logan 1986; Scholz 1990). During the interseismic period, stress accumulation and elastic deformation of the crust around major fault planes can induce microseismic activity within rock volumes of the order of a few tens of cubic kilometres. Zones where microseismic activity is likely to be concentrated are the process zones near the extremities of major fault planes where stresses accumulate (Cottrell 1964), or highly fractured regions located above ductile shear zones. Microseismicity may also represent internal deformation of blocks bounded by large faults (Fuchs *et al.* 1987; Jackson & White 1989; Echtler, Lüchen & Mayer 1994).

If the occurrence of microevents is controlled by a pre-existing network of fractures near major fault planes, where stresses may be locally modified, then some focal mechanisms may not be consistent with those expected from the large-scale tectonics. This is the case for the reverse and the few strike-slip events observed (e.g. events 8, 39, 79, 86, 294; Appendices C and D). All of these events are compatible with minimum horizontal (compressive) stress oriented N–S. However, modification of stresses may also be transient, for instance in response to slip episodes on major faults (e.g. Lyon-Caen *et al.*

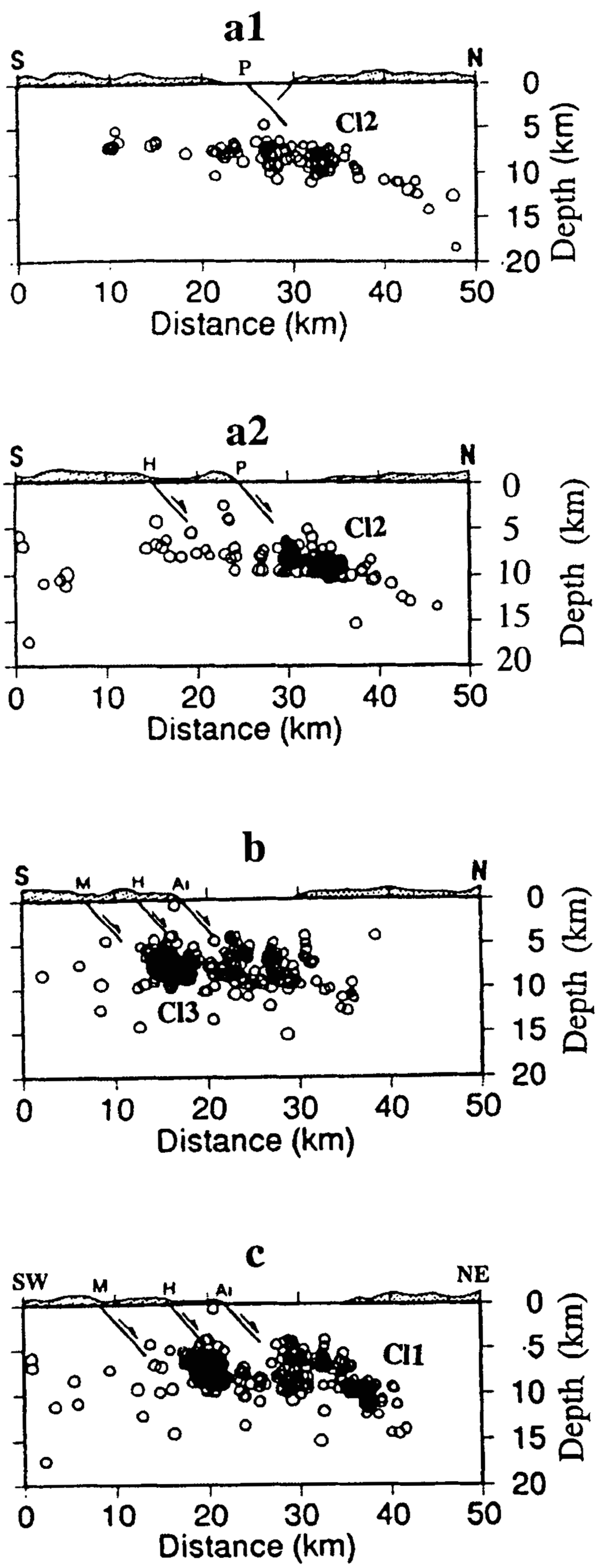

Figure 10. Vertical sections of seismicity (see Fig. 8 for location), with no vertical exaggeration. The half-width of projection is 6 km. Active faults observed at the surface have been extrapolated to a depth of 5 km with a dip of 50°. P: Psathopyrgos fault; H: Helike fault, Ai: Aigion fault; M: Mamousia fault.

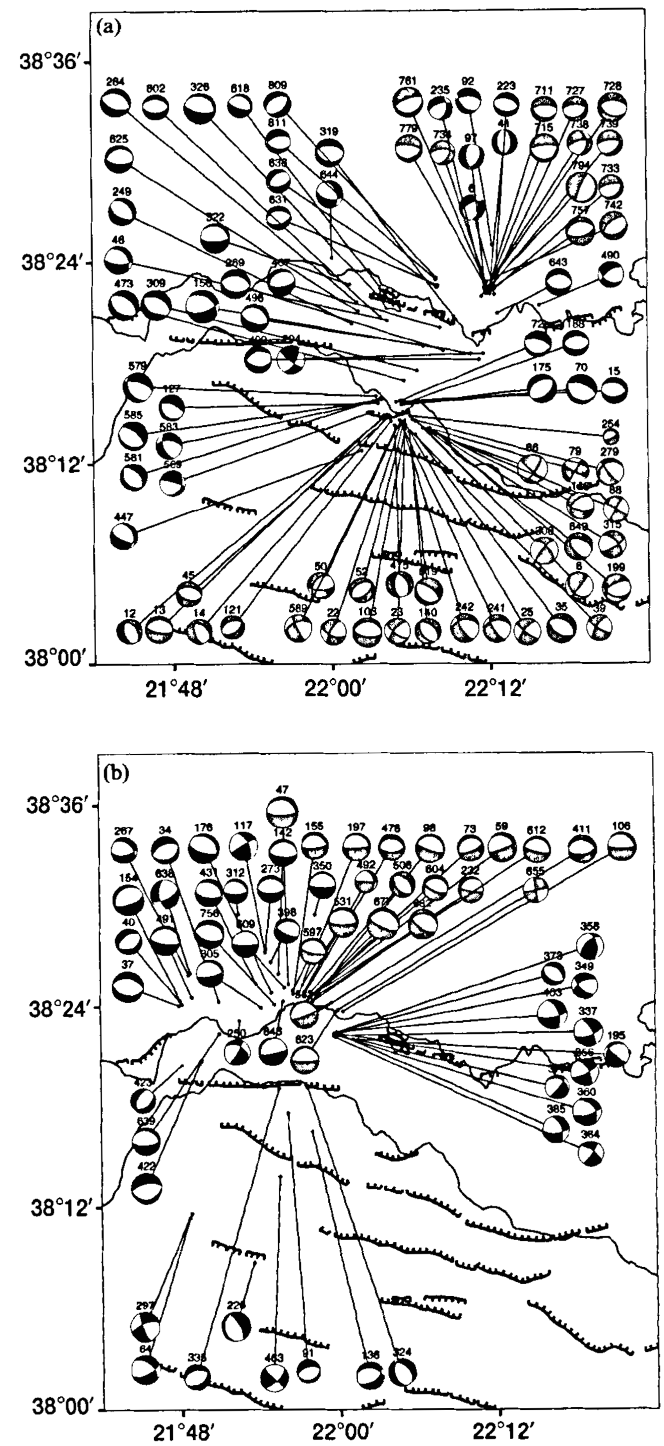

Figure 11. Maps with the 148 calculated fault-plane solutions. The size of the sphere (lower hemisphere) is proportional to magnitude. Grey fault-plane solutions are those within the three main clusters Cl1, Cl2 and Cl3. (a) Focal mechanisms in the western part of the network. (b) Focal mechanisms in the eastern part of the network. Numbers refer to events in Appendices B and C.

1988). This may be the case for cluster Cl1, which represents aftershocks of the $M_L = 4.5$ earthquake of July 3, 1991.

The two sections in Fig. 12 show the observed seismicity and some representative fault-plane solutions, with the geological information. In the western part of the network (section a, Fig. 12) the distribution of the seismicity with depth increasing towards the north is consistent with the gently north-dipping nodal planes of the focal mechanisms (events 312, 491, 639, 677) and with the mean P and T axes of cluster Cl2. A likely interpretation is that a low-angle normal fault or a detachment zone occurs between 9 and 11 km depth, dipping north at about 15°. The seismicity could also be associated with slip on small antithetic faults corresponding to the nodal planes dipping steeply to the south. However, a network of such antithetic faults with the geometry given by the observed seismicity distribution may also accommodate overall strain compatible with the proposed detachment zone. If the dip of the Psathopyrgos fault decreases from 50° as observed at the surface to less steep values at depth, then it would connect with the detachment in the region of cluster Cl2. The intersection of the two fault zones would be a likely place for increased fracturing and thus for generating microseismic activity. The possible upward and downward extensions of the proposed detachment are difficult to define due to the lack of observed microevents. Nevertheless, it seems likely that the detachment extends down-dip to the north, dying out in the ductile lower part of the crust, where it would become aseismic.

The relationship between the spatial event distribution, the focal mechanisms and the surface geology in the eastern part of the network (section b, Fig. 12) appears to be more complex than to the west. The occurrence of a detachment on section b can only be justified by the geometry of the observed seismicity and would correspond to the lower limit of the seismogenic layer. This lower limit appears to dip gently northwards, although no determined fault-plane solution is

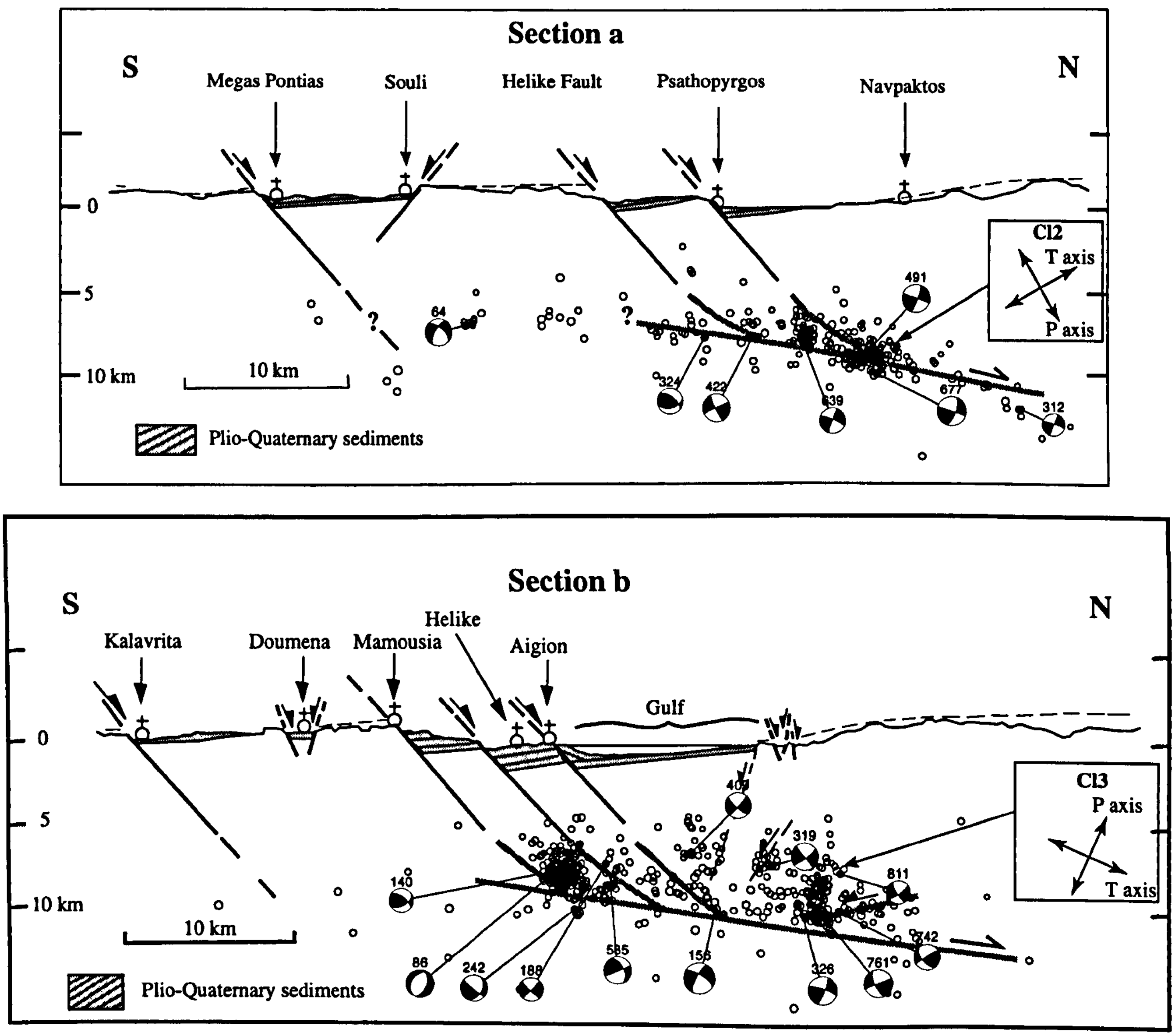

Figure 12. Interpretative sections (locations in Fig. 1). Only a few representative fault-plane solutions have been projected on the vertical plane. Insets represent mean P and T axes for clusters Cl2 and Cl3. The active major normal faults documented at the surface connect with the northward-dipping plane (shaded), consistent with the spatial distribution of seismicity and the gently north-dipping nodal planes of the western focal mechanisms.

clearly associated with it. As in section a, the major active normal faults documented at the surface (the Mamousia, Helike and Aigion faults) may connect with the hypothetical detachment at depth. Small antithetic faults probably related to flexure of the hanging wall have been recognized in the field (Fig. 1). Because the total amount of N–S extension is greater in section b than in section a, the hanging wall (northern part of the Gulf) may also be more fractured (Rigo 1994; Armijo *et al.* 1996). Part of the observed shallow (0–15 km) seismicity in the hanging wall of the Helike–Aigion faults could be associated with such flexure-related antithetic faulting, in agreement with the 60°–65° south-dipping nodal planes of some mechanisms (dashed lines in section b, Fig. 12). Farther north in the hanging wall, cluster Cl3 is located at an average depth of about 10 km. The mean P axis of cluster Cl3 is steeper than those of clusters Cl1 and Cl2 (Figs 12, 10 and 9). Also, unlike the other two clusters, the mean T axis of cluster Cl3 plunges to the north (Table 2; Fig. 12, section b). Cluster Cl3 may thus be associated with gently south-dipping faulting above the detachment. Finally, the Aigion cluster (Cl1, Fig. 9) is located roughly in the region where the downward extension of the Mamousia fault may connect with the proposed detachment (Fig. 12). However, the seismicity associated with this cluster appears to diffuse over almost all of the lower part of the block bounded by the Mamousia and the Helike faults.

5 CONCLUSIONS

Because of the high resolution of the data presented here, we can provide a precise, instantaneous image of the deforming study area. This high resolution enables us to describe precisely the mechanisms of small earthquakes and to draw some inferences about the large-scale geometry and mechanics of extension in the Gulf of Corinth. The data set suggests the existence, beneath the Gulf of Corinth, of a detachment zone that contributes significantly to the overall deformation process. All the large active normal faults mapped appear to connect downwards with the proposed detachment at around 10 km depth. The geometry of the detachment would be that of a normal fault dipping 15° ($\pm 10°$) northwards, as revealed by the studied seismicity. This is similar to the geometry and mechanism suggested by King *et al.* (1985) for the eastern part of the Corinth Gulf in the Corinth–Perachora region.

Except for cluster Cl2, the observed cluster activity does not exhibit a simple geometry associated with any particular fault. Fault-plane solutions can be quite varied within one cluster, as in the Aigion cluster (Cl1). The cluster microearthquake activity is likely to be mostly located on small structures, antithetic faults or fracture zones located near the extremities of the large faults.

To evaluate roughly the total seismic moment released by the 774 well-located events in the network, we use the formula relating the magnitude M_L to the seismic moment M_0 established in the Volos region in Central Greece ($\log M_0 = 1.5\ M_L + 9.0$; Makropoulos, personal communication). The total seismic moment released during the 30 day period is of the order of $0.3–3.0 \times 10^{16}$ N m, which corresponds to an event with an M_s of 4.3–4.9. This represents quite a high rate of diffuse deformation which is unlikely to be a permanent feature. Previous seismicity experiments in the area indicate activity beneath the Gulf between Patras and Aigion (Melis *et al.* 1989) and on the northern side of the Gulf (Hatzfeld *et al.* 1990). Because the resolution of these studies is much poorer than the one presented here, it is difficult to make valid comparisons. However, it appears that the Aigion cluster Cl1 was not active at the time of these experiments (1983–84 and 6 weeks during 1986). Thus, the cluster activity probably changes with time, contributing to the redistribution of stress at some depth. In the Gulf of Corinth, the focal depths of large earthquakes occur near the base of the seismogenic layer at 10–15 km depth, as in other regions under extension throughout the world (Sibson 1982; Meissner & Strehlau 1982; Jackson & White 1989). Therefore, we suggest that the microseismic activity observed corresponds to episodes of stress transfer from the lower semi-brittle zone to the upper brittle zone, through slip on a detachment zone. This process may cause stresses to concentrate in regions near the base of the large steep faults seen at the surface. Such regions are likely places for large normal-faulting earthquakes to initiate their rupture. However, our observations do not tell us if this activity represents to some extent the initiation of a preseismic stage. That the microseismic activity is most probably transient suggests that the stress accumulation near the large faults may operate in cycles with small spatial extent and short duration which may only correspond to discrete episodes during the main seismic cycle.

ACKNOWLEDGMENTS

The authors thank all the participants of the summer 1991 field experiment. We also thank Geneviève Patau for reading some of the seismograms, Bertrand Meyer for helpful discussions and Kurt Feigl for a helpful reading of manuscript. The Direction aux Risques Majeurs (DRM) and Institut National des Sciences de l'Univers (INSU) provided financial support. We also benefited from EEC EPOCH Programme support. This is IPGP contribution no. 1427.

REFERENCES

Abers, G., 1991. Possible seismogenic shallow-dipping normal faults in the Woodlark–D'entrecasteaux extensional province, Papua New Guinea, *Geology,* **19,** 1205–1208.

Ambraseys, N.N. & Jackson, J.A., 1990. Seismicity and associated strain of Central Greece between 1890 and 1988, *Geophys. J. Int.,* **101,** 663–708.

Amorese, D., 1993. Sismotectonique et déformation actuelle de la terminaison nord occidentale de l'Arc Égéen (Iles Ioniennes, Acharnanie, Épire, Grèce), *Thèse de Doctorat de 3ème cycle,* Université Joseph Fourier, Grenoble, France.

Arabasz, W.J. & Julander, D.R., 1986. Geometry of seismically active faults and crustal deformation within the Basin and Range—Colorado Plateau transition in Utah, *Spec. Pap. Geol. Soc. Am.,* **208,** 43–74.

Armijo, R., Meyer, B., King, G.C.P., Rigo, A. & Papanastassiou, D., 1996. Quaternary evolution of the Corinth Rift and its implications for the Late Cenozoic evolution of the Aegean, *Geophys. J. Int.,* **126,** 11–53

Bernard, P. & Zollo, A., 1989a. The Irpinia (Italy) 1980 earthquake: detailed analysis of a complex normal fault, *J. geophys. Res.,* **94,** 1631–1647.

Bernard, P. & Zollo, A., 1989b. Inversion of near source S polarization for parameters of double couple point sources, *Bull. seism. Soc. Am.,* **79,** 1779–1809.

Booth, D.C. & Crampin, S., 1985. Shear wave polarizations on a curved wavefront at an isotropic free surface, *Geophys. J. R. astr. Soc.*, **88**, 31–45.

Bouin, M.P., Téllez, J. & Bernard, P., 1996. Seismic anisotropy around the Gulf of Corinth, Greece, deduced from three-component seismograms of local earthquakes and its relationship with crustal strain, *J. geophys. Res.*, **101**, 5797–5811.

Brillinger, D.R., Udias, A. & Bolt, B.A., 1980. A probability model for regional focal mechanism solutions, *Bull. seism. Soc. Am.*, **70**, 149–170.

Briole, P., Deschamps, A., Lyon-Caen, H., Papazissi, K. & Martinod, J., 1993. The Itea ($M_S=5.9$) earthquake of November 18, 1992. Characteristics of the main shock inferred from body waves and ground displacement analysis, *Proc. 2nd Cong. of the Hellenic Geophys. Un. in Florina*, **1**, 297–308.

Chester, F.M. & Logan, J.M., 1986. Implications for mechanical properties of brittle faults from observations of the Punchbowl fault zone, California, *Pageoph.*, **124**, 79–106.

Cottrell, A.H., 1964. *The Mechanical Properties of Materials*, John Wiley and Sons, New York, NY.

Covington, H.R., 1983. Structural evolution of the Raft River Basin, Idaho, *Geol. Soc. Am. Memoir*, **157**, 229–237.

De Chabalier, J.B., Lyon-Caen, H., Zollo, A., Deschamps, A., Bernard, P. & Hatzfeld, D., 1992. A detailed analysis of microearthquakes in western Crete from digital three-component seismograms, *Geophys. J. Int.*, **110**, 347–360.

Echtler, H.P., Lüschen, E. & Mayer, G., 1994. Lower crustal thinning in the Rhinegraben: Implications for recent rifting, *Tectonics*, **13**, 342–353.

Evans, R., 1984. Effects of the free surface on shear wavetrains, *Geophys. J. R. astr. Soc.*, **76**, 165–172.

Eyidogan, H. & Jackson, J., 1985. A seismological study of normal faulting in the Demirci, Alasehir and Gediz earthquakes of 1969–70 in western Turkey: implications for the nature and geometry of deformation in the continental crust, *Geophys. J R. astr. Soc.*, **81**, 569–607.

Fuchs, K., Bonjer, K.-P., Gajewski, D., Lüschen, E., Prodehl, C., Sandmeier, K.-J., Wenzel, F. & Wilhelm, H., 1987. Crustal evolution of the Rhinegraben area. 1. Exploring the lower crust in the Rhinegraben rift by unified geophysical experiments, *Tectonophysics*, **141**, 261–275.

Galanopoulos, A.G., 1960. Greece, a catalogue of shocks with $I_0 \geq$ VI or $M \geq 5$ for the years 1801–1958, Academy of Science, Athens.

Galanopoulos, A.G., 1961. Greece, a catalogue of shocks with $I_0 \geq$ VII for the years prior to 1800, Academy of Science, Athens.

Hatzfeld, D., Pedotti, G., Hatzidimitriou, P. & Makropoulos, K., 1990. The strain pattern in the Western Hellenic Arc deduced from a microearthquake survey, *Geophys. J. Int.*, **101**, 181–202.

Jackson, J.A. & White, N.J., 1989. Normal faulting in the upper continental crust: observations from regions of active extension, *J. Struct. Geol.*, **11**, 15–36.

Jackson, J.A., Gagnepain, J., Houseman, G., King, G.C.P., Papadimitriou, P., Soufleris, C. & Virieux, J., 1982. Seismicity, normal faulting and the geomorphological development of the Gulf of Corinth (Greece): the Corinth earthquakes of February and March 1981, *Earth planet. Sci. Lett.*, **57**, 377–397.

Jones, H.C., 1987. A geophysical and geological investigation of extensional structures, Great Basin, Western United States, *PhD thesis*, Massachusetts Institute of Technology, Cambridge, MA.

King, G.C.P., Ouyang, Z.X., Papadimitriou, P., Deschamps, A., Gagnepain, J., Houseman, G., Jackson, J.A., Soufleris, C. & Virieux, J., 1985. The evolution of the Gulf of Corinth (Greece): an aftershock study of the 1981 earthquakes, *Geophys. J. R. astr. Soc.*, **80**, 677–683.

King, G.C.P., Oppenheimer, D. & Amelung, F., 1994. Block versus continuum deformation in the western United States, *Earth planet. Sci. Lett.*, **128**, 55–64.

Lee, W.H.K. & Lahr, J.C., 1975. HYPO71 (revised): a computer program for determining hypocenter, magnitude and first motion pattern of local earthquakes, *US Geol. Survey Open-File report*, **75–311**, 116 pp.

Le Meur, H., 1994. Tomographie tridimensionnelle à partir des temps des premières arrivées des ondes P et S, application à la région de Patras, *Thèse de Doctorat de 3ème cycle*, Université Paris 7, France.

Logatchev, N.A. & Zorin, Y.A., 1987. Evidence and causes of the two-stages development of the Baïkal rift, *Tectonophysics*, **143**, 225–234.

Lyon-Caen, H., Armijo, R., Drakopoulos, J., Baskoutas, J., Delibassis, N., Gaulon, R., Kouskouna, V., Latoussakis, J., Makropoulos, K., Papadimitriou, P., Papanastassiou, D., Pedotti, G., 1988. The 1986 Kalamata (South Peloponnesus) earthquake: detailed study of a normal fault and tectonic implications, *J. geophys. Res.*, **93**, 14 967–15 000.

Maier, L. & Eisbacher, G.H., 1991. Crustal kinematics and deep structure of the northern Rhine Graben, Germany, *Tectonics*, **10 (3)**, 621–630.

Meissner, R. & Strehlau, J., 1982. Limits of stress in continental crust and their relation to the depth–frequency relation of shallow earthquakes, *Tectonics*, **1**, 73–89.

Melis, N.S., Brooks, M. & Pearce, R.G., 1989. A microearthquake study in the Gulf of Patras region, western Greece, and its seismotectonic interpretation, *Geophys. J. R. astr. Soc.*, **98**, 515–524.

Papazachos, B. & Papazachos, K., 1989. *The Earthquakes in Greece*, Thessaloniki, Ziti Publications, Greece (in Greek).

Rigo, A., 1994. Étude sismotectonique et géodésique du Golfe de Corinthe (Grèce), *Thèse de Doctorat de 3ème cycle*, Université Paris 7, France.

Schmidt, J.F.J., 1881. *Studien über Vulkans und Erdbeben*, C. Scholtze, Leipzig (in German).

Scholz, C.H., 1990. *The Mechanics of Earthquakes and Faulting*, Cambridge University Press, Cambridge.

Sibson, R.H., 1982. Fault zone models heat flow and depth distribution of earthquakes in the continental crust of the United States, *Bull. seism. Soc. Am.*, **72**, 151–163.

Taymaz, T., Jackson, J. & McKenzie, D., 1991. Active tectonics of the north and central Aegean Sea, *Geophys. J. Int.*, **106**, 433–490.

Wenzel, F., Brun, J.P. & ECORS-DEKORP working group, 1991. A deep reflection seismic line across the northern Rhine Graben, *Earth planet. Sci. Lett.*, **104**, 140–150.

Zollo, A. & Bernard, P., 1991. Fault mechanisms from near source data: joint inversion of S polarizations and P polarities, *Geophys. J. Int.*, **104**, 441–451.

APPENDIX A: COORDINATES OF STATIONS DURING THE 1991 EXPERIMENT

Sites	latitude (°N)	longitude (°E)	Sites	latitude (°N)	longitude (°E)
daph	38°25.27'	22°06.21'	marn	38°24.66'	21°49.71'
pyrg	38°24.64'	22°00.99'	pale	38°30.02'	21°50.70'
kout	38°24.04'	22°13.07'	eupa	38°26.13'	21°55.36'
varn	38°27.88'	21°57.58'	iaso	38°13.68'	21°48.94'
trik	38°26.76'	21°54.20'	mira	38°09.31'	21°51.10'
triz	38°21.79'	22°04.30'	arra	38°15.96'	21°58.96'
scal	38°25.24'	21°50.48'	piti	38°15.97'	21°53.90'
neok	38°29.30'	21°50.48'	anoz	38°18.76'	21°56.89'
velv	38°23.38'	21°45.98'	arak	38°08.10'	21°57.44'
avor	38°28.04'	22°08.23'	liko	38°13.44'	21°56.60'
rig1	38°28.83'	21°46.05'	mamo	38°09.41'	22°07.92'
rig2	38°28.21'	21°44.84'	taxi	38°10.71'	22°02.42'
thio	38°29.52'	22°00.08'	kefa	38°11.24'	21°49.59'
tolo	38°22.41'	22°11.37'	tran	38°15.74'	21°51.12'
psar	38°19.51'	22°11.07'	kmri	38°13.42'	22°02.23'
limn	38°32.45'	21°58.01'	pant	38°08.48'	22°03.67'
dori	38°30.81'	22°09.61'	ptge	38°11.47'	22°06.22'
pano	38°22.97'	22°16.30'	krin	38°11.54'	21°57.11'
vrai	38°26.99'	22°11.24'	derv	38°10.31'	22°08.24'
poti	38°28.77'	22°04.43'	agge	38°12.97'	22°05.20'
palp	38°28.77'	21°52.70'	rodo	38°15.65'	22°01.71'
pits	38°25.93'	21°44.89'	akas	38°16.62'	21°50.76'
krok	38°31.87'	22°04.27'	dafn	38°12.49'	22°00.30'
mala	38°26.38'	22°15.16'	fter	38°09.36'	22°04.61'
elai	38°23.36'	22°07.08	argi	38°16.96'	21°51.56'
kmro	38°24.70'	21°56.93'	univ	38°17.32'	21°47.33'
klim	38°25.21'	21°58.09'	rodi	38°19.42'	21°53.87'
palr	38°27.78'	21°52.23'	laka	38°14.67'	21°58.76'
sote	38°25.66'	22°10.71'	koul	38°14.33'	22°05.18'
kamb	38°27.20'	22°00.54'	koun	38°11.19'	22°00.72'
kali	38°23.61'	22°08.45'	mal1	38°22.37'	21°52.68'
serg	38°24.82'	22°03.43'	mal2	38°22.81'	21°54.22'

APPENDIX B: EVENT LOCATIONS FROM HYPO71.

Time origin time (h mn s); Lat.: latitude N (°mn); Long.: longitude E (°mn); depth in km; ERZ: precision on the focal depth in km; Mag.: Magnitude Ml; RMS: Root Mean Square of the computed location in sec; ERX and ERY precision on the epicentral position in km.

Date	Time	Lat	Long	Depth	ERZ	Mag.	RMS	ERX	ERY	n.evt
910801	1 1033.17	38 20.62	22 12.32	7.69	0.3	2.08	0.06	0.4	0.3	1
910801	1 1038.81	38 15.38	22 5.60	8.24	0.6	2.20	0.09	0.3	0.4	2
910801	1 5135.29	38 11.69	21 49.08	5.23	0.7	2.26	0.13	0.6	0.4	5
910801	2 3610.60	38 22.12	22 12.47	11.21	0.3	2.37	0.08	0.2	0.3	6
910801	6 630.14	38 14.71	22 6.40	5.74	0.8	2.52	0.13	0.4	0.4	7
910801	8 1438.00	38 14.27	22 6.80	7.04	0.2	2.60	0.12	0.3	0.3	8
910801	10 45 0.32	38 14.00	22 6.23	6.78	0.3	2.23	0.12	0.3	0.3	9
910801	10 5358.15	38 13.61	22 6.39	7.22	0.5	2.59	0.16	0.3	0.4	10
910801	13 1226.25	38 33.95	21 54.19	17.61	1.0	2.64	0.07	0.3	0.8	11
910801	13 4610.04	38 14.98	22 4.29	7.76	0.5	2.33	0.12	0.3	0.3	12
910801	13 4645.20	38 14.87	22 3.97	8.33	0.6	2.54	0.17	0.3	0.3	13
910801	13 48 0.25	38 14.84	22 4.24	8.11	0.5	2.33	0.12	0.3	0.4	14
910801	13 4816.05	38 15.73	22 4.96	6.09	1.1	2.48	0.26	0.6	0.6	15
910801	15 4137.04	38 14.21	22 5.45	7.31	0.6	2.49	0.18	0.4	0.4	16
910801	15 4534.15	38 22.23	22 0.74	8.03	0.6	2.12	0.14	0.5	0.4	17
910801	15 52 1.90	38 18.34	22 8.30	8.03	0.5	2.48	0.12	0.5	0.8	18
910801	15 5922.99	38 14.72	22 5.03	6.11	0.9	2.09	0.16	0.5	0.5	19
910801	16 818.77	38 13.89	22 6.34	7.39	0.7	2.18	0.16	0.8	0.6	20
910801	16 1623.79	38 13.80	22 6.75	7.09	0.5	2.44	0.12	0.3	0.4	21
910801	16 2155.67	38 14.55	22 5.36	6.48	0.3	2.45	0.13	0.2	0.2	22
910801	16 2231.80	38 14.64	22 5.60	6.98	0.3	2.42	0.15	0.3	0.3	23
910801	16 53 0.12	38 14.56	22 5.80	5.77	0.6	2.36	0.13	0.4	0.3	24
910801	19 137.72	38 14.42	22 5.65	7.16	0.3	2.50	0.15	0.3	0.3	25
910801	19 4915.54	38 17.19	22 2.57	8.50	1.6	2.41	0.17	0.6	0.6	27
910801	20 624.16	38 14.74	22 4.24	8.10	0.5	2.33	0.13	0.3	0.3	28
910801	21 53 4.85	38 18.75	22 10.94	7.17	0.2	2.51	0.08	0.4	0.5	30
910801	21 5728.87	38 17.84	22 10.20	8.47	1.6	2.55	0.16	0.6	0.8	31
910801	22 732.61	38 11.63	21 48.76	6.78	0.4	2.21	0.12	0.5	0.4	32
910801	22 5956.04	38 18.77	22 4.25	8.70	0.6	2.68	0.12	0.2	0.2	33
910801	23 8 4.59	38 24.28	21 50.94	9.79	0.4	2.62	0.10	0.2	0.2	34
910801	23 4460.00	38 13.75	22 6.43	7.64	0.3	2.77	0.14	0.2	0.2	35
910802	0 1724.67	38 20.74	21 46.57	9.07	0.5	2.93	0.15	0.3	0.2	36
910802	0 3640.40	38 24.03	21 47.94	9.09	0.6	2.93	0.20	0.5	0.4	37
910802	0 3640.48	38 23.99	21 48.10	9.29	0.8	2.86	0.05	0.4	0.2	38
910802	0 5235.45	38 14.33	22 5.65	7.54	0.4	2.43	0.13	0.2	0.2	39
910802	1 1128.11	38 24.12	21 48.17	8.24	0.3	2.47	0.08	0.3	0.2	40
910802	2 3918.92	38 22.64	22 12.09	9.61	0.2	2.39	0.10	0.2	0.2	41
910802	2 40 6.52	38 11.57	21 48.86	7.15	0.3	2.64	0.13	0.5	0.4	42
910802	4 4255.96	38 18.14	22 9.02	4.17	0.6	2.11	0.05	0.6	0.5	43
910802	5 710.42	38 21.60	22 11.47	8.95	0.4	2.42	0.13	0.4	0.2	44
910802	7 1936.83	38 14.86	22 4.46	7.66	0.4	2.38	0.13	0.2	0.2	45
910802	7 2444.15	38 20.56	22 4.30	9.80	0.9	2.63	0.20	0.3	0.3	46
910802	9 21 8.71	38 25.34	21 56.21	9.84	0.2	2.91	0.10	0.1	0.1	47
910802	9 5651.16	38 25.46	21 55.84	8.86	0.3	2.52	0.05	0.1	0.2	48
910802	11 4324.26	38 11.87	21 48.69	6.46	0.5	2.70	0.12	0.6	0.4	49

Date	Time	Lat	Long	Depth	ERZ	Mag.	RMS	ERX	ERY	n.evt
910802	13 2216.11	38 14.61	22 5.30	7.32	0.4	2.50	0.14	0.2	0.2	50
910802	13 3255.62	38 14.57	22 5.53	7.43	0.4	2.35	0.10	0.3	0.2	52
910802	13 5252.37	38 14.28	22 4.34	5.20	1.2	2.26	0.22	0.6	0.6	53
910802	13 54 3.07	38 14.41	22 6.58	6.93	1.0	2.46	0.14	0.4	0.4	54
910802	14 332.54	38 14.77	22 5.81	5.58	0.6	2.15	0.09	0.3	0.3	55
910802	14 456.33	38 14.46	22 5.30	6.24	0.6	2.35	0.14	0.4	0.3	56
910802	15 2136.86	38 24.04	21 52.61	7.66	0.4	2.38	0.06	0.2	0.2	57
910802	17 5847.76	38 14.28	22 5.73	6.82	0.6	2.37	0.16	0.4	0.4	58
910802	18 31 0.52	38 24.74	21 58.13	10.18	0.3	2.72	0.12	0.1	0.2	59
910802	19 5 9.59	38 21.71	22 13.86	11.65	0.4	2.47	0.11	0.5	0.4	60
910802	19 4122.67	38 18.35	22 10.45	7.50	0.3	2.96	0.15	0.3	0.1	61
910802	19 5337.05	38 15.01	22 4.88	6.37	0.9	2.22	0.09	0.6	0.7	62
910802	20 27 8.75	38 14.91	22 4.42	7.14	0.2	2.54	0.12	0.2	0.2	63
910802	21 38 2.25	38 11.34	21 48.67	7.18	0.3	2.78	0.17	0.5	0.4	64
910802	21 4125.64	38 23.21	22 9.61	9.29	0.5	2.39	0.10	0.5	0.4	65
910802	21 5714.18	38 14.74	22 5.53	5.61	0.5	2.32	0.13	0.3	0.2	66
910802	22 1722.32	38 14.65	22 6.59	7.44	0.7	2.49	0.14	0.5	0.4	67
910802	22 2513.36	38 15.36	22 5.45	8.61	1.0	2.20	0.16	0.4	0.5	68
910802	22 2935.94	38 19.21	22 10.24	5.81	0.3	2.26	0.05	0.4	0.2	69
910802	23 29 4.44	38 15.55	22 5.40	9.00	0.5	2.83	0.16	0.2	0.2	70
910802	23 33 5.85	38 15.45	22 5.30	8.33	0.8	2.35	0.14	0.4	0.3	71
910803	2 059.76	38 15.79	22 5.30	8.91	0.6	2.40	0.13	0.3	0.3	72
910803	2 1449.37	38 24.38	21 57.68	9.23	0.5	2.45	0.10	0.2	0.2	73
910803	2 3534.77	38 14.25	22 4.86	7.31	0.8	2.38	0.17	0.4	0.5	74
910803	3 2011.57	38 15.90	22 5.14	8.25	1.2	2.46	0.18	0.5	0.6	75
910803	4 25 2.84	38 21.15	21 44.38	8.99	0.4	2.86	0.08	0.3	0.1	78
910803	4 5838.55	38 14.13	22 7.37	6.18	0.5	2.47	0.15	0.3	0.2	79
910803	7 636.62	38 22.26	22 12.40	11.24	0.3	2.45	0.09	0.3	0.3	80
910803	7 1344.71	38 18.17	21 48.52	8.28	0.7	2.51	0.10	0.6	0.3	81
910803	8 325.60	38 15.01	22 4.84	8.14	0.5	2.41	0.10	0.3	0.3	82
910803	8 551.52	38 14.98	22 4.74	7.91	1.0	2.01	0.14	0.9	0.7	83
910803	8 3121.36	38 14.25	22 7.24	6.73	0.4	2.37	0.15	0.7	0.5	84
910803	8 5428.27	38 14.06	22 8.12	8.11	0.9	2.58	0.13	0.8	0.6	85
910803	9 458.56	38 13.90	22 7.52	7.34	0.3	2.78	0.15	0.2	0.2	86
910803	10 056.76	38 19.31	22 6.18	9.64	0.5	2.42	0.06	0.2	0.3	87
910803	11 5149.59	38 14.02	22 7.36	6.82	0.3	2.47	0.13	0.3	0.2	88
910803	11 5332.80	38 22.20	22 11.78	9.19	0.2	2.24	0.04	0.2	0.2	89
910803	11 5634.55	38 22.27	22 11.65	9.10	0.2	2.21	0.04	0.2	0.2	90
910803	12 2457.48	38 17.55	21 56.12	7.96	0.4	2.23	0.13	0.4	0.3	91
910803	12 3454.06	38 25.04	22 12.26	13.81	0.2	2.46	0.07	0.2	0.2	92
910803	12 4716.16	38 18.14	21 47.74	7.92	0.5	2.26	0.09	0.6	0.4	93
910803	12 5720.68	38 23.76	22 3.33	10.17	0.4	2.37	0.09	0.2	0.4	94
910803	14 1023.49	38 14.35	21 58.28	6.76	0.3	2.57	0.11	0.2	0.2	95
910803	14 2333.03	38 18.47	22 9.70	4.05	0.5	2.02	0.08	0.5	0.2	96
910803	16 1931.41	38 22.38	22 11.74	9.70	0.3	2.37	0.08	0.2	0.2	97
910803	18 1418.27	38 24.82	21 57.92	9.59	0.5	2.66	0.09	0.1	0.2	98
910803	19 33 8.51	38 19.13	22 9.53	6.07	0.5	2.46	0.12	0.4	0.3	99
910803	19 749.47	38 18.89	21 49.73	7.72	1.4	2.37	0.22	0.8	0.5	100
910803	19 33 8.49	38 19.18	22 9.61	6.43	0.4	2.46	0.13	0.4	0.2	101
910803	20 2149.26	38 22.08	21 49.62	7.07	0.2	2.30	0.07	0.2	0.1	102
910803	20 4447.74	38 14.10	22 5.60	7.72	0.3	2.73	0.13	0.2	0.2	103
910803	22 5 2.92	38 18.74	21 48.35	6.99	0.2	2.36	0.05	0.3	0.1	104

APPENDIX B (*Continued.*)

Date	Time	Lat	Long	Depth	ERZ	Mag.	RMS	ERX	ERY	n.evt
910803	23 1747.65	38 16.61	22 6.36	10.33	0.6	2.40	0.09	0.3	0.3	105
910803	23 1817.88	38 23.72	22 0.38	9.29	0.3	2.67	0.11	0.1	0.1	106
910803	23 3916.24	38 14.41	22 5.94	8.77	1.4	2.31	0.22	0.8	1.0	107
910803	23 4025.11	38 18.14	22 9.63	6.14	0.7	2.51	0.17	0.7	0.3	108
910804	0 57 9.15	38 11.30	21 48.45	7.00	0.4	2.42	0.12	0.4	0.4	109
910804	1 4713.44	38 20.72	22 1.76	9.47	0.6	2.58	0.06	0.2	0.2	110
910804	2 3222.04	38 19.59	22 9.44	9.43	0.6	2.44	0.11	0.3	0.2	112
910804	3 1333.92	38 22.47	22 11.90	9.69	0.4	2.35	0.09	0.3	0.3	113
910804	3 3613.17	38 21.96	22 2.05	8.25	0.3	2.16	0.04	0.2	0.2	114
910804	3 5621.77	38 21.86	21 44.47	8.57	0.1	2.34	0.02	0.2	0.1	115
910804	8 4326.36	38 18.43	21 47.63	7.71	0.3	2.60	0.08	0.2	0.1	116
910804	9 5721.25	38 27.24	21 54.52	10.51	0.3	2.66	0.09	0.1	0.2	117
910804	11 1345.82	38 25.20	21 51.00	8.16	0.6	2.10	0.09	0.3	0.4	120
910804	11 2319.88	38 14.59	22 4.56	6.81	0.5	2.21	0.12	0.2	0.3	121
910804	12 1221.65	38 18.37	22 8.45	5.36	0.6	2.11	0.08	0.5	0.5	122
910804	14 053.81	38 33.19	21 53.87	17.88	0.3	2.58	0.08	0.2	0.3	123
910804	16 17 3.98	38 24.72	21 57.69	9.90	0.3	2.73	0.10	0.1	0.1	125
910804	16 38 0.44	38 30.47	21 43.43	19.56	1.0	2.47	0.12	1.0	0.9	126
910804	17 1542.97	38 15.62	22 3.58	7.29	0.4	2.42	0.11	0.2	0.2	127
910804	18 5254.19	38 27.59	21 49.31	10.78	0.3	2.38	0.08	0.2	0.2	129
910804	19 3939.89	38 22.27	21 53.12	6.73	1.2	2.27	0.14	0.4	0.4	130
910804	20 1637.49	38 20.76	21 49.09	7.27	1.5	2.38	0.23	0.9	0.5	131
910804	20 3925.47	38 14.17	22 6.82	7.56	0.7	2.38	0.12	0.5	0.5	132
910804	20 5419.35	38 14.28	22 4.90	7.42	0.5	2.43	0.16	0.4	0.4	133
910804	21 4139.73	38 6.47	21 57.19	6.89	2.5	2.63	0.20	0.6	1.4	134
910804	22 5748.97	38 19.02	22 9.71	5.65	0.5	2.37	0.11	0.3	0.4	135
910804	23 2253.89	38 16.44	21 57.98	5.51	0.4	2.61	0.11	0.2	0.2	136
910805	0 219.19	38 20.00	21 49.47	6.54	0.5	2.58	0.09	0.3	0.3	137
910805	0 2534.59	38 14.43	22 7.20	7.86	0.4	2.49	0.11	0.2	0.2	138
910805	0 26 9.24	38 21.28	21 45.09	9.25	0.6	2.60	0.13	0.4	0.2	139
910805	0 5127.11	38 13.96	22 5.94	7.18	0.3	2.38	0.17	0.3	0.4	140
910805	2 852.85	38 13.81	22 7.31	7.91	0.7	2.34	0.15	0.4	0.4	141
910805	2 4654.52	38 25.97	21 55.47	10.00	0.3	2.63	0.10	0.1	0.1	142
910805	3 121.92	38 14.18	22 5.30	7.11	0.5	2.42	0.14	0.3	0.5	143
910805	3 1232.47	38 20.45	22 9.44	6.72	0.3	2.28	0.10	0.3	0.3	144
910805	3 20 0.11	38 20.71	22 9.42	6.78	0.3	2.54	0.13	0.2	0.2	145
910805	3 51 1.78	38 14.07	22 7.50	7.50	0.3	2.55	0.12	0.2	0.2	146
910805	4 1512.81	38 20.69	22 9.62	4.75	0.2	2.04	0.03	0.1	0.1	147
910805	5 2238.26	38 21.12	22 8.53	9.14	0.3	2.25	0.07	0.2	0.2	148
910805	5 4753.96	38 18.25	22 11.16	6.20	0.6	2.35	0.22	0.6	0.5	149
910805	10 1145.48	38 20.28	22 9.19	6.55	0.2	2.23	0.05	0.2	0.2	152
910805	11 16 2.98	38 19.62	22 14.76	10.52	0.4	2.30	0.07	0.4	0.4	153
910805	12 2135.11	38 24.34	21 48.01	9.31	0.3	2.94	0.08	0.2	0.1	154
910805	13 657.17	38 24.76	21 56.57	9.28	0.4	2.49	0.09	0.1	0.2	155
910805	14 313.67	38 19.04	22 7.03	9.35	0.4	3.12	0.10	0.2	0.1	156
910805	14 27 8.47	38 19.14	22 5.09	6.60	2.3	2.19	0.19	0.8	0.6	157
910805	17 3513.61	38 22.06	22 0.76	8.60	0.6	2.00	0.06	0.3	0.5	160
910805	18 5149.07	38 25.43	21 54.61	8.49	0.4	2.53	0.06	0.2	0.2	161
910805	19 11 7.23	38 18.57	22 9.71	5.63	0.5	2.23	0.10	0.4	0.4	162
910805	20 119.25	38 14.41	22 4.88	7.84	0.5	2.51	0.12	0.2	0.3	163
910805	20 521.84	38 14.21	22 4.89	8.38	0.6	2.90	0.12	0.2	0.2	164
910805	20 1544.23	38 14.39	22 4.66	7.77	0.6	2.31	0.11	0.2	0.4	169
910805	20 1557.47	38 17.16	22 5.42	13.46	1.3	2.47	0.13	0.7	0.7	170
910805	21 4730.93	38 26.80	22 4.77	4.07	0.7	2.47	0.09	0.3	0.5	173
910805	21 57 6.99	38 20.86	21 48.65	7.09	0.2	2.63	0.12	0.3	0.2	174
910805	22 415.95	38 15.56	22 5.33	8.75	0.7	2.73	0.15	0.2	0.2	175
910805	22 59 4.96	38 24.83	21 54.94	9.43	0.3	2.82	0.10	0.1	0.1	176
910806	0 915.41	38 23.66	22 0.92	8.78	0.4	0.00	0.06	0.2	0.5	177
910806	0 4646.43	38 14.53	22 6.89	7.90	0.3	2.50	0.11	0.2	0.2	178
910806	0 52 5.03	38 24.67	21 57.62	8.69	0.4	2.43	0.08	0.2	0.2	179
910806	1 5710.94	38 20.43	21 49.13	4.66	0.9	2.52	0.09	0.3	0.4	180
910806	2 2537 76	38 18.37	22 9.84	10.62	0.6	2.87	0.11	0.2	0.1	181
910806	6 2757.26	38 14.57	22 4.37	7.75	0.5	2.73	0.09	0.4	0.4	183
910806	6 3940.03	38 14.49	22 7.17	4.71	2.2	2.32	0.12	0.4	0.5	184
910806	7 3724.29	38 18.72	22 6.81	8.32	0.5	2.53	0.10	0.2	0.1	185
910806	8 416.73	38 18.54	22 7.08	7.99	0.7	2.03	0.08	0.4	0.4	186
910806	9 2948.51	38 15.58	22 5.49	6.75	0.8	2.42	0.12	0.2	0.2	188
910806	10 0 6.85	38 14.37	21 57.91	4.33	0.7	2.99	0.11	0.4	0.3	190
910806	10 151.62	38 15.60	22 5.26	8.03	0.4	2.49	0.12	0.3	0.2	191
910806	11 3134.02	38 15.83	22 4.90	7.69	0.6	2.32	0.12	0.3	0.2	193
910806	11 4138.86	38 15.70	22 5.08	8.10	0.5	2.56	0.14	0.2	0.3	194
910806	12 1015.50	38 22.02	22 1.08	8.31	0.3	2.47	0.07	0.1	0.1	195
910806	13 2727.06	38 24.72	21 56.96	8.85	0.8	2.57	0.13	0.1	0.2	197
910806	13 2727.21	38 24.60	21 56.73	8.52	0.2	0.00	0.02	0.1	0.2	198
910806	14 1658.96	38 14.17	22 7.50	7.39	0.4	2.70	0.13	0.2	0.2	199
910806	15 27 2.00	38 14.27	22 4.85	8.15	0.4	2.67	0.15	0.3	0.3	200
910806	15 27 0.63	38 12.87	22 4.19	14.22	0.5	2.78	0.08	0.4	0.3	201
910806	15 28 5.11	38 14.43	22 5.01	7.81	0.3	2.53	0.10	0.2	0.2	202
910806	15 2842.06	38 14.37	22 4.95	7.89	0.3	2.49	0.11	0.2	0.2	203
910806	15 4121.26	38 20.72	21 49.43	7.18	0.2	2.70	0.09	0.3	0.1	204
910806	18 556.47	38 14.43	22 5.07	7.55	1.5	2.25	0.13	0.6	0.7	207
910806	21 5157.82	38 17.70	21 47.59	7.67	0.4	2.47	0.09	0.4	0.2	208
910806	22 253.31	38 23.23	21 48.22	7.87	0.7	2.42	0.14	0.5	0.5	210
910806	22 1231.10	38 23.23	22 0.26	8.07	0.4	0.00	0.06	0.2	0.2	211
910806	23 744.15	38 11.49	21 49.12	7.06	0.2	2.82	0.13	0.3	0.3	213
910806	23 3720.67	38 14.45	22 5.15	7.20	0.3	2.55	0.14	0.2	0.3	214
910807	0 1020.65	38 18.17	22 9.66	3.96	0.3	2.12	0.10	0.3	0.2	215
910807	0 2740.30	38 21.59	22 3.95	8.45	0.3	2.19	0.08	0.1	0.2	216
910807	0 5241.54	38 15.48	22 5.28	6.62	2.9	0.00	0.25	1.1	0.7	217
910807	1 628.62	38 15.59	22 5.41	8.29	0.6	2.40	0.14	0.3	0.3	218
910807	1 4321.26	38 15.15	22 6.01	8.81	1.7	2.45	0.21	0.7	0.6	219
910807	2 736.16	38 15.58	22 6.14	8.23	1.6	2.78	0.23	0.7	0.6	220
910807	3 3943.35	38 22.09	22 1.09	8.21	1.3	0.00	0.15	0.9	0.6	221
910807	4 48 5.67	38 23.66	22 0.74	7.84	0.5	2.03	0.09	0.5	0.9	222
910807	7 2253.10	38 22.42	22 12.46	11.13	0.4	2.36	0.14	0.4	0.2	223
910807	9 734.00	38 18.08	22 10.33	6.21	0.4	2.14	0.07	0.7	0.5	224
910807	11 1318.39	38 8.73	21 53.46	10.56	0.3	2.74	0.10	0.2	0.3	226
910807	12 430.79	38 23.37	22 16.10	13.33	0.4	2.28	0.05	0.6	0.4	228
910807	13 3258.01	38 24.92	21 55.93	8.31	0.8	0.00	0.08	0.4	0.2	229
910807	14 5915.42	38 5.54	21 47.03	18.24	0.6	0.00	0.13	0.6	0.7	230
910807	15 4548.20	38 15.82	22 1.58	8.10	0.6	2.46	0.11	0.5	0.3	231
910807	15 5033.71	38 24.30	21 58.09	9.43	0.4	2.38	0.10	0.2	0.2	232
910807	19 3341.32	38 20.36	22 11.80	6.96	0.3	2.14	0.05	0.3	0.2	233
910807	21 5835.40	38 22.07	21 47.24	8.35	0.6	2.03	0.07	0.4	0.6	234

APPENDIX B (*Continued.*)

Date	Time	Lat	Long	Depth	ERZ	Mag.	RMS	ERX	ERY	n.evt
910807	22 2017.05	38 22.50	22 11.64	10.32	0.2	2.30	0.07	0.2	0.2	235
910807	23 5913.23	38 13.89	22 7.22	8.26	0.6	2.39	0.16	0.4	0.4	236
910808	2 2512.14	38 16.12	22 10.38	7.27	0.9	2.25	0.08	0.9	0.4	237
910808	2 5757.85	38 20.81	22 2.88	8.41	0.5	2.32	0.06	0.2	0.2	238
910808	4 753.43	38 24.24	21 59.15	9.12	0.4	2.35	0.07	0.3	0.4	239
910808	4 11 9.73	38 13.90	22 7.60	8.45	1.4	2.45	0.17	0.8	0.5	240
910808	4 1435.76	38 14.65	22 5.18	9.71	0.7	2.63	0.18	0.3	0.3	241
910808	4 1558.69	38 14.59	22 5.28	9.45	0.5	2.70	0.14	0.2	0.2	242
910808	10 5926.80	38 37.16	22 9.81	17.08	1.6	2.48	0.10	0.8	1.2	243
910808	13 5147.83	38 14.60	22 6.20	8.17	0.7	0.00	0.08	0.3	0.5	246
910808	13 5935.04	38 14.43	22 4.97	7.85	0.3	2.61	0.11	0.2	0.2	247
910808	14 2649.75	38 17.11	22 7.85	8.34	0.8	2.60	0.14	0.4	0.2	248
910808	16 1545.86	38 20.40	22 1.60	9.45	0.4	2.54	0.10	0.2	0.1	249
910808	16 5924.85	38 23.11	21 52.49	8.22	0.7	2.45	0.13	0.3	0.3	250
910808	18 31 8.67	38 22.57	21 55.42	8.46	0.6	2.46	0.12	0.2	0.2	251
910808	19 22 3.69	38 21.38	22 14.38	10.76	0.3	2.80	0.12	0.3	0.2	252
910808	20 319.46	38 19.05	22 2.27	8.95	0.4	2.78	0.09	0.2	0.1	253
910808	20 5814.07	38 14.88	22 5.99	8.05	0.3	0.00	0.07	0.2	0.2	254
910808	20 5827.4	38 14.91	22 6.08	8.15	0.3	2.73	0.11	0.2	0.2	255
910808	21 1227.67	38 24.58	21 48.84	8.38	0.2	2.31	0.05	0.2	0.2	257
910808	21 55 0.92	38 14.29	22 4.89	7.14	0.4	2.45	0.15	0.3	0.3	258
910809	1 36 6.45	38 24.15	22 12.46	9.46	0.9	2.22	0.13	0.6	0.8	259
910809	2 533.32	38 14.25	22 6.08	9.93	1.0	0.00	0.10	0.4	0.5	260
910809	2 1941.53	38 14.65	22 6.32	9.09	1.0	0.00	0.08	0.3	0.4	261
910809	2 48 9.55	38 18.47	22 10.03	6.23	0.5	2.41	0.17	0.4	0.3	262
910809	3 5837.62	38 15.19	21 52.90	8.04	0.3	2.63	0.13	0.2	0.2	263
910809	6 1811.28	38 21.68	22 2.01	9.48	0.4	2.77	0.12	0.1	0.1	264
910809	7 1124.61	38 23.67	22 0.63	8.17	0.2	2.47	0.05	0.2	0.4	266
910809	10 3 9.46	38 25.89	21 48.66	9.45	0.2	2.46	0.05	0.1	0.2	267
910809	10 23 7.89	38 18.60	22 9.75	4.66	0.6	1.92	0.08	0.4	0.5	268
910809	11 56 5.24	38 18.77	22 8.50	7.13	0.2	2.71	0.12	0.2	0.1	269
910809	12 031.26	38 24.96	21 53.54	9.06	1.0	0.00	0.11	0.6	0.5	270
910809	12 623.41	38 24.71	21 53.92	8.90	0.7	0.00	0.11	0.4	0.4	271
910809	13 2120.48	38 21.50	21 59.85	7.72	0.2	0.00	0.02	0.1	0.2	272
910809	14 930.15	38 27.43	21 54.55	10.24	0.3	2.54	0.10	0.2	0.3	273
910809	14 4216.59	38 20.72	22 0.52	7.39	0.4	2.53	0.11	0.3	0.2	274
910809	16 1911.88	38 24.91	21 57.12	9.14	0.4	2.25	0.08	0.3	0.3	275
910809	16 3322.08	38 24.26	21 50.94	8.27	0.5	2.65	0.09	0.2	0.3	276
910809	16 3514.21	38 24.25	21 51.06	7.28	0.3	2.16	0.05	0.1	0.3	277
910809	17 1646.53	38 14.83	22 6.01	9.18	0.6	2.68	0.15	0.3	0.2	278
910809	17 2653.04	38 14.69	22 6.18	9.79	0.5	2.59	0.11	0.2	0.2	279
910809	18 2738.05	38 19.24	21 46.94	8.74	0.9	2.54	0.14	0.5	0.3	280
910809	18 3428.40	38 25.03	21 57.29	9.04	0.4	2.44	0.09	0.2	0.2	282
910809	20 1914.51	38 14.24	22 4.85	7.64	0.6	2.35	0.17	0.4	0.4	283
910809	21 154.15	38 20.61	22 1.59	11.91	0.7	0.00	0.12	0.4	0.3	285
910809	21 156.07	38 20.72	22 1.88	8.22	0.8	2.43	0.13	0.3	0.2	286
910809	21 4246.25	38 20.10	22 6.18	9.55	0.8	2.34	0.07	0.2	0.2	288
910809	22 4659.30	38 24.17	21 58.04	9.48	0.7	2.24	0.12	0.3	0.5	290
910809	22 55 3.47	38 14.50	22 4.66	7.13	0.4	2.52	0.18	0.3	0.4	291
910809	23 1135.51	38 24.87	21 57.05	8.56	0.4	2.13	0.06	0.3	0.2	292
910809	23 5022.63	38 21.54	21 51.02	7.12	0.2	1.02	0.07	0.3	0.2	293
910810	2 31 4.86	38 18.59	22 11.57	6.95	0.3	2.67	0.15	0.4	0.2	294

Date	Time	Lat	Long	Depth	ERZ	Mag.	RMS	ERX	ERY	n.evt
910810	5 2515.48	38 14.08	22 5.75	7.49	0.5	2.38	0.10	0.4	0.4	295
910810	5 5042.11	38 19.27	22 9.48	5.10	1.5	2.51	0.21	0.5	0.4	296
910810	6 4039.00	38 11.60	21 48.78	6.95	0.2	2.79	0.10	0.4	0.2	297
910810	6 4927.92	38 14.20	22 5.77	7.16	1.0	2.21	0.20	0.8	0.9	298
910810	7 1322.15	38 14.81	22 5.86	6.73	0.5	2.50	0.17	0.4	0.4	299
910810	8 2941.75	38 9.04	21 54.93	11.23	0.6	2.61	0.15	0.3	0.5	301
910810	9 41 3.20	38 20.70	22 9.49	6.64	0.4	2.47	0.07	0.2	0.3	302
910810	9 5515.09	38 20.91	22 9.16	5.98	0.5	2.29	0.10	0.3	0.4	303
910810	10 740.83	38 24.87	21 57.10	8.67	0.4	2.12	0.05	0.2	0.3	304
910810	10 1535.73	38 23.94	21 54.15	8.98	0.5	2.56	0.12	0.2	0.2	305
910810	10 4227.95	38 13.91	22 7.37	7.04	0.4	2.61	0.17	0.3	0.4	308
910810	12 3259.56	38 17.59	22 6.59	8.36	0.6	2.85	0.11	0.2	0.1	309
910810	13 026.16	38 20.57	21 57.14	8.00	0.3	2.92	0.11	0.2	0.1	310
910810	14 9 1.51	38 14.48	22 5.13	5.53	0.7	2.28	0.09	0.4	0.2	311
910810	14 40 3.30	38 29.50	21 52.45	12.34	0.6	2.28	0.15	0.3	0.4	312
910810	15 1951.41	38 20.68	21 57.31	9.46	0.9	2.77	0.24	0.5	0.4	313
910810	15 2247.60	38 21.26	21 44.46	10.64	0.7	2.79	0.16	0.5	0.2	314
910810	17 4426.29	38 14.08	22 7.44	7.52	0.4	2.62	0.13	0.3	0.3	315
910810	18 3917.03	38 14.74	22 5.06	5.64	0.6	2.36	0.11	0.3	0.2	316
910810	21 5039.64	38 14.38	22 6.11	7.06	0.3	2.37	0.13	0.3	0.3	318
910810	22 26 0.27	38 19.41	22 9.79	7.15	0.7	0.00	0.08	0.8	0.8	320
910810	22 3742.65	38 14.64	22 4.99	7.33	0.5	2.57	0.17	0.3	0.3	321
910810	22 4756.56	38 22.71	22 1.47	9.65	0.4	2.79	0.12	0.1	0.1	322
910810	23 3321.53	38 14.19	22 5.75	7.44	0.4	2.17	0.09	0.4	0.3	323
910811	0 54 0.08	38 19.09	21 57.65	8.02	0.3	2.59	0.14	0.2	0.1	324
910811	0 5921.00	38 28.33	21 48.85	11.02	0.4	2.30	0.09	0.3	0.3	325
910811	2 3129.49	38 21.73	22 4.02	9.09	0.4	2.92	0.13	0.2	0.1	326
910811	2 50 1.43	38 20.88	21 47.04	8.08	0.6	2.75	0.15	0.5	0.3	327
910811	4 729.23	38 20.55	22 12.22	8.30	0.4	2.47	0.07	0.4	0.5	328
910811	4 2129.34	38 13.87	22 6.10	7.19	0.4	2.41	0.11	0.5	0.4	329
910811	4 4018.90	38 14.48	22 4.86	6.42	0.7	2.23	0.12	0.4	0.3	330
910811	4 4923.28	38 14.09	22 6.13	8.16	0.5	2.52	0.14	0.4	0.4	331
910811	10 5031.72	38 9.37	22 2.42	7.27	0.4	2.42	0.07	0.3	0.4	332
910811	14 42 6.34	38 27.65	22 1.77	8.52	0.4	1.92	0.07	0.2	0.4	333
910811	15 1427.30	38 22.30	21 59.55	8.12	0.2	2.83	0.13	0.1	0.1	334
910811	15 5348.44	38 19.07	21 55.46	9.50	0.6	2.47	0.17	0.3	0.3	335
910811	15 5711.40	38 19.16	21 55.29	9.43	0.4	0.00	0.06	0.6	0.3	336
910811	16 218.06	38 22.24	21 59.60	7.96	0.2	2.73	0.15	0.1	0.1	337
910811	16 546.52	38 22.43	21 59.74	8.09	0.2	2.43	0.09	0.1	0.1	338
910811	16 1017.00	38 20.49	22 9.63	5.66	0.3	1.92	0.04	0.2	0.1	339
910811	16 2329.71	38 22.54	21 59.95	7.71	0.7	2.33	0.10	0.2	0.3	340
910811	16 4434.18	38 20.53	22 9.53	5.38	0.3	1.92	0.04	0.1	0.1	341
910811	17 345.18	38 22.38	21 59.64	7.58	0.7	2.33	0.09	0.2	0.2	342
910811	17 1733.50	38 22.33	21 59.54	7.44	0.5	2.35	0.13	0.3	0.2	343
910811	19 1541.49	38 20.37	22 8.94	6.15	0.9	2.32	0.16	0.4	0.4	345
910811	19 3316.55	38 22.44	21 59.73	7.58	0.5	2.50	0.12	0.2	0.2	348
910811	20 26 1.44	38 22.35	21 59.72	7.69	0.3	2.46	0.10	0.2	0.2	349
910811	22 2135.96	38 29.46	21 58.27	12.76	0.6	2.48	0.15	0.2	0.4	350
910811	23 3815.47	38 22.32	21 59.75	8.10	0.5	2.76	0.18	0.3	0.2	351
910812	0 1343.36	38 22.32	21 59.68	7.27	0.7	2.20	0.07	0.2	0.2	352
910812	0 2723.25	38 24.46	21 57.90	9.49	0.3	2.67	0.11	0.1	0.1	353
910812	0 3258.21	38 22.30	21 59.85	7.85	0.5	0.00	0.14	0.2	0.4	354

APPENDIX B (*Continued.*)

Date	Time	Lat	Long	Depth	ERZ	Mag.	RMS	ERX	ERY	n.evt
910812	0 45 1.66	38 22.38	21 59.78	7.56	0.4	2.44	0.10	0.2	0.2	355
910812	0 4745.08	38 22.38	21 59.77	8.55	0.3	2.59	0.11	0.1	0.1	356
910812	0 5546.56	38 15.65	22 5.66	8.00	0.4	2.38	0.08	0.3	0.2	357
910812	1 22 9.25	38 22.39	21 59.81	7.85	0.3	2.57	0.10	0.1	0.1	358
910812	1 3944.15	38 22.31	21 59.75	7.78	0.4	2.42	0.11	0.2	0.2	359
910812	1 4847.36	38 22.26	21 59.87	8.17	0.2	2.64	0.11	0.1	0.1	360
910812	3 859.34	38 23.25	22 0.05	9.52	1.4	2.65	0.23	0.6	0.6	361
910812	3 2031.93	38 22.46	21 59.73	6.85	0.4	2.40	0.10	0.2	0.2	362
910812	3 5345.19	38 13.15	22 3.40	9.47	0.6	2.54	0.16	0.3	0.3	363
910812	4 26 3.51	38 22.16	21 59.74	7.47	0.5	2.40	0.15	0.3	0.2	364
910812	4 57 8.24	38 21.17	22 2.04	8.55	0.3	2.51	0.07	0.1	0.1	365
910812	5 738.19	38 22.67	21 46.15	8.65	0.3	2.83	0.11	0.2	0.2	366
910812	5 13 7.68	38 24.80	21 57.21	8.89	0.4	2.37	0.10	0.2	0.2	367
910812	5 2927.39	38 21.78	22 15.95	12.08	0.5	2.52	0.17	0.6	0.4	368
910812	6 020.35	38 22.63	21 59.96	8.21	0.8	2.38	0.14	0.4	0.5	369
910812	6 1351.81	38 22.44	21 59.72	8.05	0.3	2.37	0.13	0.2	0.2	370
910812	6 4748.54	38 17.23	22 4.40	9.69	0.9	2.46	0.17	0.4	0.3	371
910812	7 25 4.12	38 22.16	22 1.58	8.78	0.3	2.42	0.08	0.2	0.1	372
910812	7 55 7.39	38 22.38	21 59.64	8.57	0.5	2.20	0.04	0.2	0.2	373
910812	7 5917.59	38 14.24	22 5.96	7.42	0.5	2.46	0.13	0.4	0.3	374
910812	9 343.44	38 22.47	22 0.18	7.92	0.9	0.00	0.12	0.4	0.5	375
910812	9 1942.10	38 22.49	21 59.80	7.50	0.5	0.00	0.08	0.2	0.2	376
910812	9 5045.48	38 21.98	22 1.46	8.38	0.3	2.32	0.09	0.2	0.2	377
910812	9 5256.67	38 25.79	21 49.06	9.13	0.5	2.14	0.09	0.3	0.4	378
910812	11 452.58	38 22.66	21 59.75	7.24	0.4	0.00	0.08	0.3	0.2	379
910812	13 3555.73	38 14.45	22 7.25	7.58	0.5	2.52	0.11	0.3	0.2	380
910812	13 3650.81	38 35.75	22 8.68	12.44	0.9	2.20	0.05	0.3	0.6	381
910812	14 3244.75	38 14.73	22 6.22	7.40	0.4	2.69	0.12	0.2	0.2	382
910812	15 3315.19	38 23.34	22 0.60	9.57	0.3	2.69	0.09	0.1	0.1	383
910812	15 5457.03	38 23.91	21 48.24	8.12	0.3	2.65	0.10	0.2	0.2	384
910812	16 4436.87	38 22.40	21 59.79	8.47	0.3	2.57	0.08	0.1	0.1	385
910812	16 5828.49	38 18.26	22 10.03	6.13	0.5	2.35	0.10	0.6	0.5	386
910812	17 335.74	38 16.70	22 1.15	7.77	0.5	2.39	0.15	0.4	0.3	387
910812	17 813.00	38 20.01	22 5.85	9.08	0.6	2.57	0.17	0.3	0.2	388
910812	17 1637.93	38 22.24	22 13.03	11.64	0.7	2.22	0.14	0.9	0.5	389
910812	17 4130.22	38 22.49	21 59.63	8.13	0.3	2.20	0.06	0.2	0.2	390
910812	18 2245.59	38 22.34	21 59.31	6.82	0.4	0.00	0.04	0.2	0.1	391
910812	18 27 0.18	38 22.38	21 59.48	6.79	0.7	2.20	0.09	0.3	0.2	392
910812	18 2829.71	38 20.54	22 9.42	6.40	0.3	2.25	0.08	0.2	0.3	393
910812	19 051.69	38 20.92	22 9.58	6.78	0.2	2.60	0.13	0.3	0.2	394
910812	20 1750.04	38 20.55	22 9.42	6.44	0.4	2.31	0.12	0.3	0.3	395
910812	20 3945.11	38 20.65	22 9.30	6.22	0.4	2.28	0.11	0.3	0.3	396
910812	20 5513.37	38 7.63	22 1.42	10.90	0.7	2.50	0.12	0.4	0.9	397
910812	21 3925.45	38 26.67	21 54.91	9.56	0.3	2.37	0.08	0.2	0.2	398
910812	22 035.12	38 22.65	21 59.82	7.45	0.5	2.34	0.12	0.3	0.3	399
910812	22 1025.05	38 20.28	22 9.57	6.89	0.3	2.29	0.09	0.3	0.3	400
910812	23 2320.24	38 33.03	21 52.88	17.28	0.4	2.11	0.05	0.5	1.1	401
910812	23 2819.44	38 23.67	21 57.58	5.91	0.7	2.57	0.11	0.2	0.4	402
910812	23 3532.51	38 22.46	21 59.87	8.50	0.4	2.84	0.14	0.2	0.1	403
910812	23 42 2.80	38 22.29	22 0.06	8.00	0.7	2.44	0.14	0.3	0.4	404
910813	0 525.03	38 22.52	21 59.73	7.46	0.6	0.00	0.08	0.2	0.3	405
910813	0 29 2.50	38 20.55	22 9.56	6.88	0.2	2.38	0.09	0.3	0.3	406

Date	Time	Lat	Long	Depth	ERZ	Mag.	RMS	ERX	ERY	n.evt
910813	1 553.75	38 14.30	22 5.28	7.78	0.4	2.31	0.10	0.4	0.2	407
910813	1 12 3.56	38 22.53	21 59.74	7.54	0.3	2.58	0.07	0.1	0.1	408
910813	1 2158.36	38 18.24	22 11.27	6.05	0.4	2.56	0.15	0.5	0.3	409
910813	1 2332.62	38 20.87	21 48.34	8.00	0.2	2.94	0.11	0.2	0.1	410
910813	1 5134.79	38 23.59	21 58.23	8.69	0.3	2.61	0.09	0.1	0.1	411
910813	1 52 7.49	38 23.76	21 58.69	9.01	0.7	2.39	0.06	0.4	0.2	412
910813	3 2810.12	38 22.46	21 59.29	6.71	0.4	0.00	0.06	0.1	0.2	413
910813	3 4451.10	38 21.70	21 47.31	7.32	0.5	2.47	0.06	0.3	0.4	414
910813	3 5524.45	38 22.51	21 59.73	7.25	0.3	0.00	0.04	0.1	0.1	415
910813	10 4325.26	38 22.66	21 56.25	8.76	0.6	0.00	0.07	0.2	0.2	416
910813	11 2541.56	38 13.89	22 5.75	6.99	0.6	2.23	0.13	0.4	0.5	417
910813	12 039.19	38 20.39	22 9.82	7.20	0.4	2.09	0.09	0.3	0.4	418
910813	12 5727.45	38 22.48	21 59.78	6.06	0.5	0.00	0.06	0.3	0.2	420
910813	13 5245.34	38 13.36	22 4.52	5.38	0.5	2.27	0.07	0.3	0.4	421
910813	14 3233.17	38 20.73	21 49.62	7.95	0.4	2.87	0.12	0.3	0.3	422
910813	14 3233.10	38 20.46	21 48.14	7.13	0.2	2.40	0.06	0.3	0.3	423
910813	14 3647.37	38 24.35	21 51.07	7.69	0.3	0.00	0.07	0.2	0.3	424
910813	14 5744.32	38 22.53	22 0.28	7.82	0.5	0.00	0.12	0.3	0.5	425
910813	17 53 9.00	38 22.26	22 0.24	7.51	0.4	0.00	0.11	0.2	0.3	426
910813	19 5558.12	38 13.75	22 6.09	7.23	0.8	2.39	0.18	0.5	0.4	427
910813	20 5238.37	38 14.02	22 5.68	7.61	0.3	2.60	0.14	0.2	0.2	428
910813	21 4755.38	38 25.19	21 58.74	9.43	0.3	2.30	0.07	0.1	0.2	429
910813	23 6 8.44	38 22.03	22 10.92	8.57	0.5	2.02	0.07	0.5	0.3	430
910813	23 1048.02	38 25.34	21 53.77	8.52	0.3	2.63	0.08	0.1	0.1	431
910813	23 2754.59	38 14.04	22 7.72	7.65	0.9	2.39	0.13	0.6	0.5	432
910813	23 4954.00	38 19.57	22 8.77	8.09	0.5	2.41	0.15	0.3	0.2	433
910813	23 50 9.97	38 20.83	22 13.26	6.86	0.2	2.11	0.05	0.3	0.2	434
910814	1 2618.84	38 22.02	22 11.29	9.07	0.3	1.92	0.04	0.4	0.2	436
910814	2 1245.27	38 20.13	22 8.28	8.21	0.3	2.54	0.10	0.2	0.1	437
910814	2 1914.93	38 22.45	22 0.09	7.85	0.4	0.00	0.13	0.3	0.5	438
910814	2 2822.46	38 23.07	22 0.71	8.24	0.5	0.00	0.12	0.3	0.6	439
910814	2 5923.08	38 22.62	22 0.07	8.27	0.3	2.12	0.10	0.1	0.2	440
910814	3 2 3.71	38 24.91	21 58.22	10.23	0.6	2.33	0.12	0.2	0.3	441
910814	7 457.56	38 22.95	22 16.02	12.27	1.2	0.00	0.14	1.0	1.3	443
910814	8 414.41	38 20.56	22 9.45	6.22	0.4	0.00	0.06	0.2	0.3	444
910814	8 414.40	38 20.55	22 9.43	5.99	0.3	2.41	0.04	0.2	0.2	445
910814	8 437.81	38 21.58	22 8.76	9.07	0.4	1.79	0.05	0.2	0.2	446
910814	9 44 3.17	38 12.79	22 2.32	9.79	0.4	2.53	0.14	0.2	0.3	447
910814	14 3831.21	38 24.32	21 59.73	9.09	0.3	2.38	0.06	0.2	0.2	449
910814	15 1639.94	38 33.70	22 4.06	13.42	0.5	2.74	0.12	0.2	0.5	450
910814	15 1937.89	38 34.09	22 4.16	13.76	0.7	2.12	0.13	0.3	0.5	451
910814	15 1946.02	38 33.85	22 4.23	13.18	0.6	2.62	0.12	0.3	0.5	452
910814	16 1343.50	38 14.66	22 4.34	6.96	0.3	2.58	0.15	0.3	0.2	453
910814	16 4957.90	38 13.96	22 4.49	5.72	0.5	2.37	0.12	0.3	0.3	454
910814	17 14 7.27	38 14.22	22 4.65	6.83	0.7	2.32	0.16	0.4	0.5	455
910814	19 1410.38	38 21.07	22 3.79	9.27	0.4	2.52	0.09	0.2	0.1	456
910814	19 3313.06	38 18.80	22 8.51	5.62	0.9	0.00	0.08	0.3	0.2	457
910814	23 5134.50	38 16.36	22 3.40	6.67	1.0	2.32	0.15	0.7	0.7	458
910815	1 026.89	38 21.36	22 1.84	8.29	0.6	2.48	0.13	0.3	0.3	459
910815	1 2342.42	38 14.42	22 6.15	8.78	1.0	2.38	0.13	0.5	0.4	460
910815	1 52 6.06	38 25.36	21 55.55	8.76	0.4	2.13	0.07	0.2	0.2	461
910815	2 5731.25	38 23.27	21 47.17	11.04	0.4	2.57	0.11	0.3	0.2	462

APPENDIX B (*Continued.*)

Date	Time	Lat	Long	Depth	ERZ	Mag.	RMS	ERX	ERY	n.evt
910815	5 4952.98	38 13.78	21 55.48	7.24	0.4	2.62	0.13	0.2	0.3	463
910815	5 5934.01	38 14.23	22 5.12	6.00	1.0	2.19	0.12	0.6	0.4	464
910815	6 5112.25	38 23.06	22 11.97	9.14	0.6	2.52	0.15	0.6	0.5	465
910815	7 1951.39	38 26.88	21 54.94	9.00	0.2	1.93	0.03	0.1	0.1	466
910815	8 1245.19	38 8.37	21 46.97	23.73	0.6	2.52	0.15	0.6	0.6	467
910815	10 3726.46	38 13.52	22 4.47	5.63	0.5	2.21	0.10	0.3	0.3	468
910815	10 5141.05	38 25.69	21 49.01	8.15	0.5	0.00	0.06	0.3	0.3	469
910815	13 447.40	38 21.82	22 9.22	9.53	0.7	2.15	0.10	0.6	0.4	471
910815	14 38 4.85	38 23.32	21 51.44	7.25	0.6	2.89	0.23	0.4	0.5	472
910815	15 3935.81	38 17.01	22 5.53	7.13	0.2	2.83	0.19	0.3	0.2	473
910815	15 55 1.57	38 14.34	22 4.81	6.99	0.8	2.49	0.14	0.4	0.3	475
910815	17 11 0.05	38 23.22	21 59.70	8.33	0.9	2.07	0.10	0.3	0.6	476
910815	18 44 5.19	38 15.84	22 8.41	7.85	2.6	2.12	0.15	0.9	0.5	477
910815	20 224.38	38 24.72	21 57.42	9.78	0.7	2.42	0.12	0.2	0.2	478
910815	22 1218.75	38 29.40	21 51.75	10.92	0.8	2.21	0.14	0.5	0.7	479
910815	23 042.44	38 23.70	21 59.93	9.62	0.4	2.92	0.12	0.1	0.1	480
910815	23 5317.30	38 23.14	21 45.59	9.38	0.6	2.74	0.16	0.5	0.3	481
910816	1 4340.27	38 14.25	22 5.80	8.02	0.3	2.81	0.15	0.2	0.2	482
910816	1 5611.99	38 14.25	22 5.90	8.34	0.6	2.33	0.17	0.3	0.3	483
910816	1 5951.92	38 14.48	22 5.60	8.06	0.4	2.51	0.14	0.4	0.3	484
910816	2 736.44	38 17.08	22 5.27	7.78	0.6	2.57	0.12	0.4	0.2	485
910816	3 56 4.10	38 22.65	22 13.32	12.29	0.6	2.11	0.15	0.9	0.5	486
910816	6 19 1.54	38 17.83	22 2.79	8.42	1.9	2.43	0.15	0.6	0.5	487
910816	6 4325.37	38 14.15	22 7.29	7.60	0.4	2.55	0.14	0.3	0.2	488
910816	7 5026.32	38 22.88	21 51.85	6.65	0.3	0.00	0.06	0.2	0.3	489
910816	18 19 8.46	38 21.46	22 15.81	12.22	0.3	2.44	0.10	0.3	0.2	490
910816	19 5453.38	38 24.54	21 48.90	8.79	0.4	2.86	0.16	0.4	0.2	491
910816	23 737.57	38 24.87	21 57.40	9.97	0.6	2.08	0.11	0.2	0.3	492
910817	0 3025.43	38 14.70	22 6.01	8.73	0.8	2.27	0.09	0.5	0.3	493
910817	0 3733.18	38 14.85	22 6.19	7.92	0.5	2.34	0.11	0.4	0.2	494
910817	0 4710.39	38 14.87	22 6.22	8.28	0.7	2.44	0.15	0.4	0.3	495
910817	0 5216.34	38 18.58	22 10.63	5.74	0.5	2.64	0.19	0.5	0.3	496
910817	0 5250.67	38 25.11	22 2.64	12.47	0.4	2.28	0.11	0.2	0.3	497
910817	0 5747.59	38 14.68	22 6.47	7.80	0.4	2.22	0.09	0.3	0.2	498
910817	1 2146.75	38 14.13	22 7.55	8.14	0.4	2.37	0.09	0.4	0.3	499
910817	1 4844.93	38 20.00	22 3.45	8.68	0.3	0.00	0.05	0.2	0.4	500
910817	3 543.01	38 24.66	22 7.28	12.23	0.2	2.25	0.06	0.1	0.2	501
910817	5 1359.58	38 27.16	21 54.42	8.37	0.8	2.24	0.11	0.3	0.5	502
910817	9 2010.71	38 18.18	22 10.85	8.11	0.2	2.72	0.10	0.2	0.1	503
910817	11 925.36	38 12.98	22 3.49	5.17	1.0	2.22	0.14	0.5	0.6	504
910817	14 4327.35	38 13.52	22 4.74	6.33	1.2	2.51	0.18	1.0	0.8	505
910817	14 57 7.17	38 24.36	21 58.04	9.31	0.6	2.35	0.11	0.2	0.2	506
910817	15 20 5.23	38 13.56	22 5.17	6.26	0.4	2.30	0.07	0.3	0.4	507
910817	17 3618.34	38 14.24	22 5.04	6.99	0.6	2.22	0.14	0.4	0.4	509
910817	17 3631.43	38 14.15	22 5.33	6.72	0.5	2.07	0.11	0.4	0.3	510
910817	17 3840.35	38 13.77	22 5.04	8.76	1.2	2.32	0.18	0.5	0.5	511
910817	19 1 2.95	38 19.77	22 3.40	10.00	1.3	0.00	0.16	0.7	0.5	512
910817	20 925.00	38 14.08	21 48.57	6.67	0.1	2.80	0.06	0.2	0.1	513
910817	20 1112.57	38 24.42	22 11.47	14.22	0.5	2.21	0.10	0.5	0.4	514
910817	21 849.20	38 22.09	22 1.68	9.30	0.4	2.45	0.09	0.2	0.1	515
910817	21 3718.01	38 23.44	21 57.55	8.63	0.3	2.51	0.07	0.1	0.1	516
910817	23 2429.87	38 24.67	21 53.56	8.14	0.4	2.18	0.09	0.2	0.3	517

Date	Time	Lat	Long	Depth	ERZ	Mag.	RMS	ERX	ERY	n.evt
910818	0 3244.49	38 14.26	22 5.10	7.34	0.4	2.39	0.15	0.3	0.2	519
910818	0 5939.35	38 20.92	22 1.04	7.87	0.8	0.00	0.09	0.5	0.3	520
910818	1 4030.81	38 20.81	21 48.62	6.47	0.6	0.00	0.10	0.3	0.3	521
910818	1 4036.60	38 21.40	21 48.41	5.84	0.8	0.00	0.16	0.4	0.4	522
910818	1 43 6.55	38 14.08	21 49.17	6.36	0.6	2.50	0.16	0.8	0.5	523
910818	2 1159.96	38 24.77	21 56.52	8.98	0.5	2.52	0.10	0.2	0.3	524
910818	3 4919.66	38 16.18	22 3.64	6.00	0.9	2.31	0.16	0.7	0.5	525
910818	3 50 4.45	38 18.66	21 48.76	6.66	2.2	2.35	0.21	1.4	1.9	526
910818	4 2240.86	38 14.49	22 5.33	6.97	0.4	2.32	0.11	0.2	0.2	527
910818	4 4754.56	38 20.59	21 50.65	6.46	0.6	2.43	0.11	0.3	0.3	528
910818	7 134.06	38 14.18	22 5.58	8.10	0.3	2.47	0.13	0.2	0.2	529
910818	9 5317.22	38 14.53	22 4.93	7.43	0.6	2.44	0.16	0.3	0.3	530
910818	10 3336.84	38 25.30	21 57.30	9.90	0.3	2.78	0.10	0.1	0.1	531
910818	13 4244.11	38 26.62	21 54.30	9.42	0.2	2.42	0.06	0.1	0.2	532
910818	14 3312.04	38 24.70	22 11.97	14.32	0.4	2.39	0.13	0.4	0.3	533
910818	14 4948.82	38 22.66	22 5.37	4.87	0.6	2.23	0.10	0.4	0.4	534
910818	16 2644.56	38 17.08	22 5.24	7.53	0.2	2.79	0.09	0.1	0.1	535
910818	17 41 0.10	38 13.95	22 6.12	6.58	0.6	2.29	0.10	0.3	0.2	537
910818	19 2219.62	38 13.59	22 5.96	7.65	0.8	2.58	0.12	0.6	0.6	538
910818	19 2220.19	38 14.03	22 5.97	6.00	0.9	2.42	0.15	0.8	0.6	539
910818	20 1036.17	38 18.76	22 9.86	6.25	0.7	2.12	0.16	0.9	0.9	540
910818	21 35 7.72	38 19.23	22 3.05	10.82	0.7	2.28	0.10	0.3	0.2	541
910818	21 39 9.85	38 20.80	22 12.27	9.08	0.2	2.49	0.08	0.2	0.2	542
910818	21 5615.30	38 21.09	22 12.13	9.10	0.4	2.42	0.09	0.3	0.4	543
910818	22 3357.48	38 20.70	22 12.15	8.54	0.4	2.29	0.09	0.3	0.3	544
910818	23 4 7.13	38 24.64	21 56.86	8.56	0.5	0.00	0.06	0.2	0.5	545
910818	23 3427.15	38 25.21	21 51.81	8.27	0.5	2.47	0.08	0.2	0.2	546
910819	1 1217.69	38 18.12	21 45.43	8.25	0.6	2.71	0.09	0.4	0.1	547
910819	1 3610.98	38 20.56	22 16.14	10.89	0.5	2.52	0.10	0.3	0.3	548
910819	3 5220.57	38 22.47	21 52.90	7.63	0.4	2.40	0.09	0.2	0.2	550
910819	4 4047.97	38 20.62	21 48.65	7.09	0.3	2.53	0.11	0.4	0.2	551
910819	6 750.35	38 10.65	22 3.71	9.43	0.3	2.81	0.12	0.2	0.2	552
910819	6 4249.54	38 29.44	21 52.22	12.33	0.3	2.46	0.07	0.2	0.3	553
910819	9 329.12	38 21.52	22 3.86	8.20	0.2	2.24	0.05	0.1	0.2	554
910819	9 1652.89	38 22.67	21 59.98	7.87	0.4	2.35	0.12	0.3	0.3	556
910819	10 2617.22	38 22.26	22 9.34	9.49	0.3	2.00	0.05	0.3	0.2	557
910819	10 5829.55	38 21.85	21 59.23	8.32	0.7	2.10	0.11	0.4	0.5	558
910819	12 920.60	38 31.82	21 49.40	18.36	0.4	2.12	0.08	0.3	0.5	559
910819	13 1116.07	38 19.80	22 17.76	11.76	0.6	2.19	0.11	0.7	0.6	560
910819	13 33 5.45	38 22.75	22 16.06	11.26	0.3	2.38	0.08	0.4	0.2	561
910819	14 2413.25	38 23.67	21 44.54	10.29	0.2	2.20	0.07	0.2	0.2	562
910819	16 3115.99	38 24.24	21 59.50	9.51	0.4	2.63	0.11	0.1	0.2	563
910819	18 2341.53	38 25.34	21 55.77	8.35	0.5	0.00	0.06	0.2	0.3	564
910819	20 5515.12	38 33.54	21 51.97	17.29	0.4	2.22	0.06	0.3	0.4	565
910819	23 2958.54	38 22.87	21 59.51	6.76	0.8	2.40	0.09	0.3	0.3	567
910820	0 916.27	38 6.53	21 45.41	22.04	0.4	2.92	0.13	0.4	0.4	568
910820	0 1412.06	38 15.12	22 3.06	4.70	0.3	2.42	0.09	0.2	0.2	569
910820	0 2840.64	38 18.73	21 48.43	7.28	0.3	2.61	0.12	0.3	0.2	570
910820	0 4114.47	38 6.76	21 58.40	17.28	0.9	2.45	0.14	0.6	1.1	571
910820	3 049.78	38 23.63	21 50.68	7.75	0.4	2.76	0.14	0.6	0.2	572
910820	3 941.46	38 14.44	22 4.38	7.54	0.7	2.46	0.16	0.5	0.4	575
910820	3 3658.65	38 13.90	22 3.56	6.43	0.8	2.19	0.19	0.6	0.5	576

APPENDIX B (*Continued.*)

Date	Time	Lat	Long	Depth	ERZ	Mag.	RMS	ERX	ERY	n.evt
910820	3 4036.45	38 21.79	22 12.97	11.12	0.2	2.47	0.04	0.2	0.2	577
910820	4 1818.47	38 14.54	22 4.13	7.20	0.6	2.30	0.15	0.4	0.4	578
910820	4 2241.42	38 16.05	22 3.37	7.00	0.2	2.84	0.11	0.1	0.1	579
910820	4 4358.92	38 33.46	22 5.11	13.19	0.5	2.37	0.12	0.2	0.5	580
910820	4 49 7.25	38 15.91	22 3.71	7.16	0.2	2.53	0.07	0.2	0.1	581
910820	4 5951.62	38 34.31	22 4.45	11.54	1.0	2.11	0.09	0.4	0.7	582
910820	5 3026.25	38 15.86	22 3.85	8.01	0.3	2.52	0.09	0.2	0.1	583
910820	5 4523.13	38 24.74	21 58.40	9.02	0.5	2.27	0.10	0.4	0.3	584
910820	5 50 8.81	38 15.75	22 3.15	8.04	0.3	2.75	0.19	0.2	0.2	585
910820	5 5521.89	38 14.05	22 4.05	6.33	0.4	2.43	0.07	0.3	0.4	586
910820	5 5619.63	38 15.94	22 3.35	7.04	0.2	2.63	0.06	0.2	0.1	587
910820	6 3513.45	38 23.53	21 44.88	10.31	0.2	2.40	0.05	0.2	0.2	588
910820	6 5010.20	38 14.21	22 4.97	8.43	0.5	2.61	0.16	0.3	0.2	589
910820	7 3556.85	38 14.02	22 5.98	7.49	0.5	2.27	0.11	0.3	0.2	590
910820	8 1841.70	38 23.87	22 0.30	9.08	0.5	0.00	0.07	0.3	0.3	591
910820	8 19 9.32	38 24.86	21 57.66	9.20	0.5	2.13	0.10	0.2	0.2	592
910820	8 5728.19	38 34.64	22 5.69	13.95	1.9	0.00	0.14	0.8	1.1	593
910820	10 3938.14	38 13.74	22 6.17	4.36	1.3	2.36	0.23	0.7	0.6	594
910820	13 2048.19	38 15.81	22 3.54	7.57	0.7	2.33	0.13	0.6	0.3	595
910820	13 34 8.05	38 22.00	21 59.20	8.21	0.4	2.47	0.11	0.2	0.2	596
910820	15 824.09	38 24.95	21 56.50	9.77	0.5	2.45	0.18	0.2	0.3	597
910820	18 4423.76	38 14.34	22 4.64	6.64	0.6	2.21	0.13	0.4	0.4	598
910820	19 1518.93	38 22.77	21 50.01	6.95	0.2	1.87	0.02	0.2	0.2	599
910820	19 4138.02	38 21.58	21 59.92	7.16	0.3	2.30	0.10	0.3	0.3	600
910820	23 032.81	38 22.19	21 53.39	7.46	0.3	2.39	0.10	0.2	0.2	602
910820	23 719.79	38 13.26	22 5.50	5.55	0.7	2.45	0.11	0.4	0.3	603
910821	0 328.82	38 24.53	21 57.81	9.24	0.5	2.36	0.11	0.2	0.2	604
910821	0 910.65	38 24.53	21 57.65	8.98	0.6	2.19	0.11	0.3	0.3	605
910821	0 948.86	38 24.46	21 57.90	9.22	0.4	2.53	0.13	0.2	0.2	606
910821	1 219.26	38 22.74	22 0.67	9.45	0.7	0.00	0.07	0.2	0.2	607
910821	1 4439.22	38 22.09	22 12.95	8.67	0.4	2.23	0.08	0.3	0.4	608
910821	1 5526.54	38 25.12	21 55.92	9.04	0.4	2.58	0.11	0.1	0.2	609
910821	4 3835.61	38 18.74	22 0.48	8.26	0.7	2.43	0.14	0.4	0.3	610
910821	4 5736.08	38 22.08	21 59.63	7.69	0.5	2.45	0.14	0.2	0.3	611
910821	5 32 2.00	38 24.64	21 58.38	10.34	0.5	2.48	0.18	0.3	0.3	612
910821	6 2327.60	38 25.31	22 9.74	9.33	0.7	2.47	0.09	0.5	0.6	613
910821	8 212.56	38 24.32	21 51.76	7.46	0.4	2.11	0.04	0.1	0.2	614
910821	9 33 2.53	38 23.18	21 59.57	8.42	0.6	2.34	0.13	0.3	0.4	615
910821	10 932.79	38 23.66	21 59.75	9.22	0.4	2.35	0.13	0.2	0.2	616
910821	11 5953.89	38 20.94	22 4.04	8.54	0.2	2.49	0.07	0.1	0.1	617
910821	12 216.03	38 22.05	22 4.21	9.01	0.3	2.28	0.06	0.1	0.1	618
910821	12 5 6.05	38 25.43	22 10.14	11.13	0.4	2.25	0.08	0.3	0.3	619
910821	15 2650.58	38 24.06	22 0.14	8.85	0.5	2.48	0.16	0.3	0.4	620
910821	19 4340.35	38 20.86	21 44.46	9.28	0.5	2.65	0.15	0.4	0.2	621
910821	20 42 0.78	38 22.08	21 59.10	6.33	0.8	2.24	0.11	0.3	0.2	622
910821	21 710.52	38 23.72	21 59.83	9.33	0.3	2.64	0.10	0.1	0.1	623
910821	21 1552.57	38 14.39	22 4.97	7.71	0.5	2.23	0.15	0.3	0.3	624
910821	21 3349.88	38 21.12	22 2.09	8.26	0.3	2.63	0.09	0.1	0.1	625
910821	22 1040.87	38 20.58	21 49.43	7.98	0.4	2.18	0.07	0.3	0.3	626
910821	22 3017.50	38 25.32	21 48.85	7.34	0.4	1.90	0.06	0.3	0.3	627
910821	23 2944.61	38 22.60	22 5.59	3.98	0.3	2.31	0.12	0.2	0.3	628
910821	23 4749.96	38 10.61	22 4.45	12.36	0.4	2.35	0.08	0.3	0.3	629

Date	Time	Lat	Long	Depth	ERZ	Mag.	RMS	ERX	ERY	n.evt
910821	23 5914.61	38 14.09	22 8.34	7.88	0.9	2.46	0.15	0.6	0.5	630
910822	0 1610.43	38 22.65	22 8.13	5.49	0.3	2.30	0.08	0.1	0.2	631
910822	0 2355.61	38 17.57	21 49.09	10.33	1.4	2.33	0.20	0.8	0.4	632
910822	1 3112.47	38 6.22	21 57.68	5.90	0.2	2.72	0.08	0.1	0.3	633
910822	3 3732.41	38 24.05	22 3.64	10.02	0.4	2.14	0.08	0.2	0.3	634
910822	3 4751.65	38 24.80	21 55.83	7.02	1.0	2.41	0.14	0.3	0.3	635
910822	3 5756.99	38 22.54	22 8.07	6.50	0.5	2.27	0.18	0.3	0.4	636
910822	4 2819.96	38 26.09	21 48.22	10.52	0.4	2.74	0.11	0.3	0.2	637
910822	4 2820.14	38 25.99	21 48.77	9.70	0.3	2.74	0.07	0.2	0.2	638
910822	8 3418.68	38 22.36	21 50.94	8.26	0.4	2.69	0.13	0.2	0.2	639
910822	9 1218.04	38 17.43	21 47.23	7.54	0.5	2.62	0.13	0.5	0.4	640
910822	9 32 7.48	38 21.89	21 59.61	9.69	0.8	2.17	0.09	0.3	0.3	641
910822	12 1628.95	38 20.96	22 12.66	9.97	0.3	2.48	0.10	0.3	0.2	643
910822	12 1944.41	38 24.31	22 0.14	9.55	0.2	2.53	0.07	0.1	0.1	644
910822	12 22 1.45	38 21.13	21 48.39	7.77	0.3	2.85	0.14	0.3	0.2	645
910822	14 525.97	38 22.07	21 59.67	9.67	1.1	2.21	0.13	0.4	0.4	646
910822	14 21 1.08	38 22.21	22 1.01	8.45	0.3	2.22	0.08	0.2	0.2	647
910822	15 5432.02	38 21.30	22 8.38	5.91	0.4	2.21	0.07	0.2	0.2	648
910822	16 415.65	38 14.61	22 6.43	8.82	0.5	2.61	0.12	0.2	0.2	649
910822	16 1923.24	38 17.58	21 47.03	7.71	0.4	2.52	0.06	0.3	0.2	650
910822	17 1617.59	38 18.22	22 10.02	4.50	0.6	2.45	0.13	0.4	0.2	651
910822	17 2522.71	38 18.27	22 9.89	4.60	0.7	2.52	0.16	0.5	0.3	652
910822	20 50 0.16	38 17.88	21 47.97	7.15	0.3	2.47	0.15	0.5	0.4	653
910822	21 2047.94	38 23.68	21 49.27	8.07	0.7	1.99	0.09	0.4	0.5	654
910822	21 4053.98	38 23.79	21 60.00	9.09	0.5	2.33	0.15	0.2	0.3	655
910822	21 4925.55	38 22.55	22 0.38	8.07	0.4	2.23	0.09	0.2	0.2	656
910822	22 5048.00	38 14.23	22 8.16	6.99	0.4	2.54	0.13	0.3	0.3	657
910822	23 555.87	38 25.57	22 16.37	5.40	0.8	2.46	0.09	0.5	0.8	658
910822	23 3348.37	38 14.78	22 6.58	7.74	0.5	2.48	0.13	0.2	0.2	659
910823	0 631.86	38 25.45	21 56.10	9.20	0.2	2.54	0.07	0.1	0.1	660
910823	0 5025.19	38 23.48	21 48.05	7.76	0.3	2.04	0.05	0.2	0.3	662
910823	1 1011.39	38 22.18	21 59.58	9.04	0.9	2.16	0.12	0.3	0.3	663
910823	1 1950.77	38 24.31	21 57.93	8.61	1.1	2.39	0.07	0.4	0.4	664
910823	1 3645.14	38 23.28	21 47.52	8.88	0.4	2.79	0.13	0.3	0.2	665
910823	4 5817.66	38 28.47	21 49.38	10.99	0.5	2.04	0.07	0.6	0.5	666
910823	7 3713.38	38 15.24	22 6.30	8.40	1.1	2.19	0.10	0.9	0.5	668
910823	7 3858.02	38 24.88	21 57.31	9.59	0.6	2.25	0.10	0.2	0.3	669
910823	7 3911.40	38 35.09	21 56.33	19.72	0.6	2.39	0.09	0.4	1.2	670
910823	7 4722.12	38 36.78	21 56.33	19.25	0.5	2.27	0.08	0.3	0.6	671
910823	8 2830.65	38 24.31	21 56.00	9.44	0.6	2.54	0.09	0.2	0.4	672
910823	9 2911.53	38 18.06	22 2.84	8.64	0.3	2.78	0.11	0.1	0.1	674
910823	10 4714.54	38 14.35	22 6.02	7.01	0.4	2.42	0.13	0.3	0.2	675
910823	11 1919.51	38 13.96	22 6.46	6.19	0.7	2.38	0.12	0.4	0.3	676
910823	16 4725.88	38 24.56	21 57.89	9.99	0.4	3.00	0.11	0.1	0.1	677
910823	16 4837.03	38 24.61	21 57.87	8.78	0.8	2.39	0.19	0.2	0.4	678
910823	16 4827.77	38 24.62	21 57.92	9.19	0.5	2.08	0.09	0.1	0.3	679
910823	17 2 4.11	38 25.03	21 57.92	9.27	0.6	2.49	0.13	0.2	0.3	680
910823	17 249.13	38 25.47	21 57.61	10.25	1.0	2.43	0.14	0.3	0.6	681
910823	17 439.82	38 24.57	21 57.81	9.22	0.4	2.77	0.10	0.1	0.2	682
910823	17 8 1.99	38 24.93	21 57.96	9.68	0.6	2.52	0.11	0.2	0.2	683
910823	17 2211.87	38 24.55	21 57.50	9.38	0.5	2.44	0.09	0.2	0.2	684
910823	17 2232.27	38 24.33	21 57.49	9.00	0.9	2.23	0.11	0.2	0.4	685

APPENDIX B (*Continued.*)

Date	Time	Lat	Long	Depth	ERZ	Mag.	RMS	ERX	ERY	n.evt
910823	17 2346.57	38 24.38	21 57.58	8.91	0.9	2.38	0.11	0.3	0.3	686
910823	18 5128.72	38 24.68	21 58.02	9.13	0.7	2.32	0.10	0.2	0.2	687
910823	19 12 9.01	38 24.52	21 58.53	8.11	0.4	2.31	0.09	0.5	0.6	688
910823	19 24 4.24	38 24.12	21 57.63	9.61	0.5	2.42	0.10	0.2	0.2	689
910823	19 2747.01	38 24.17	21 57.49	9.02	0.4	2.85	0.08	0.1	0.1	690
910823	19 2751.17	38 24.23	21 57.57	9.23	0.6	2.55	0.14	0.2	0.2	691
910823	20 2019.15	38 33.55	21 52.37	16.88	0.3	2.36	0.03	0.2	0.3	692
910823	20 4922.72	38 13.26	22 7.06	6.42	0.3	2.30	0.03	0.2	0.2	693
910823	21 2248.94	38 24.07	21 57.55	8.39	0.5	2.43	0.09	0.2	0.2	694
910823	21 25 7.24	38 24.00	21 57.45	9.23	0.4	2.46	0.09	0.1	0.2	695
910823	21 3059.57	38 25.27	21 59.25	8.58	0.5	2.40	0.10	0.6	0.6	696
910823	21 4157.97	38 24.92	21 58.92	8.42	0.8	2.31	0.13	0.9	1.0	697
910823	21 5332.51	38 24.42	21 57.96	9.08	0.8	2.29	0.11	0.2	0.4	698
910823	22 158.91	38 24.05	21 57.25	9.04	0.6	2.55	0.13	0.2	0.2	699
910823	22 9 1.28	38 24.08	21 57.63	8.72	0.3	2.35	0.05	0.1	0.1	700
910823	22 2140.63	38 24.09	21 57.46	9.28	0.4	2.79	0.11	0.1	0.1	701
910823	23 157.32	38 24.07	21 57.61	9.67	0.5	2.74	0.17	0.2	0.2	702
910823	23 233.62	38 23.99	21 57.42	9.65	0.6	2.83	0.19	0.2	0.2	703
910823	23 1513.05	38 23.84	21 57.77	8.99	0.5	2.27	0.08	0.2	0.2	704
910823	23 1648.37	38 24.14	21 57.74	8.99	0.5	2.58	0.10	0.2	0.2	705
910823	23 1837.94	38 24.02	21 57.67	9.17	0.4	2.43	0.09	0.1	0.1	706
910823	23 1851.74	38 23.84	21 57.64	8.87	0.5	2.54	0.13	0.2	0.2	707
910824	0 656.55	38 24.17	21 57.27	9.31	0.5	2.53	0.07	0.1	0.2	708
910824	0 918.04	38 24.16	21 57.34	9.13	0.4	2.56	0.11	0.2	0.2	709
910824	0 950.24	38 24.15	21 57.37	8.21	0.3	2.16	0.06	0.1	0.2	710
910824	0 23 2.28	38 22.23	22 11.92	9.50	0.3	2.37	0.09	0.2	0.2	711
910824	0 3126.72	38 13.83	22 5.18	7.93	0.8	2.33	0.15	0.4	0.5	712
910824	0 3711.56	38 21.96	22 11.36	9.57	0.3	2.21	0.04	0.2	0.2	713
910824	0 38 5.97	38 22.34	22 12.01	9.56	0.4	2.28	0.08	0.2	0.2	714
910824	0 39 7.86	38 22.46	22 12.05	9.35	0.3	2.64	0.08	0.2	0.2	715
910824	0 5426.01	38 35.76	21 56.38	20.06	0.5	2.51	0.08	0.3	0.6	716
910824	1 725.09	38 24.44	21 58.24	9.11	0.8	2.31	0.10	0.4	0.5	717
910824	1 746.83	38 24.29	21 57.94	9.19	0.6	2.25	0.08	0.2	0.3	718
910824	1 3732.72	38 24.29	21 57.25	8.62	0.4	2.41	0.08	0.2	0.2	719
910824	1 55 9.45	38 22.18	22 11.71	9.24	0.4	2.24	0.05	0.4	0.3	720
910824	2 7 4.53	38 22.32	22 11.77	10.03	0.4	2.46	0.08	0.3	0.6	721
910824	2 2140.27	38 22.51	22 11.80	9.30	0.3	2.92	0.08	0.2	0.3	722
910824	2 2143.41	38 22.51	22 11.90	9.70	0.3	2.47	0.09	0.2	0.3	723
910824	2 2849.54	38 22.22	22 11.85	9.57	0.4	2.43	0.09	0.3	0.5	724
910824	2 5326.63	38 22.18	22 11.89	9.57	0.4	2.30	0.08	0.2	0.2	725
910824	2 5353.18	38 22.16	22 11.82	9.52	0.5	2.19	0.09	0.3	0.3	726
910824	2 5742.49	38 22.23	22 12.08	9.08	0.4	2.31	0.09	0.3	0.3	727
910824	3 1 6.95	38 22.51	22 11.96	9.67	0.3	2.75	0.12	0.2	0.2	728
910824	4 5457.96	38 22.23	22 11.49	9.82	0.3	2.41	0.04	0.3	0.5	729
910824	5 728.32	38 22.13	22 11.85	9.90	0.2	2.21	0.07	0.2	0.2	730
910824	5 740.21	38 22.11	22 11.74	9.60	0.3	2.40	0.07	0.2	0.2	731
910824	5 825.63	38 22.86	22 11.90	9.88	0.4	2.19	0.08	0.3	0.7	732
910824	5 2217.15	38 22.15	22 12.08	9.74	0.4	2.31	0.08	0.3	0.3	733
910824	5 3629.32	38 22.25	22 12.01	9.61	0.3	2.28	0.08	0.3	0.2	734
910824	5 3852.91	38 22.17	22 11.48	10.00	0.2	2.45	0.04	0.1	0.2	735
910824	5 5016.26	38 22.24	22 11.87	9.85	0.4	2.30	0.08	0.3	0.3	736
910824	5 5058.35	38 22.47	22 12.84	9.38	0.3	2.30	0.05	0.3	0.2	737

Date	Time	Lat	Long	Depth	ERZ	Mag.	RMS	ERX	ERY	n.evt
910824	6 348.74	38 22.01	22 11.47	10.00	0.2	2.34	0.04	0.2	0.1	738
910824	6 735.73	38 22.17	22 11.82	9.81	0.4	2.44	0.08	0.2	0.2	739
910824	6 1158.37	38 21.83	22 11.17	9.88	0.3	2.23	0.06	0.3	0.2	740
910824	6 1550.23	38 22.15	22 11.67	9.67	0.4	2.37	0.09	0.3	0.5	741
910824	6 4436.57	38 22.88	22 11.84	9.43	0.4	2.62	0.11	0.3	0.3	742
910824	7 438.82	38 22.14	22 11.47	9.37	0.3	2.40	0.07	0.3	0.3	743
910824	7 3637.91	38 22.22	22 11.55	9.32	0.3	2.30	0.08	0.4	0.4	744
910824	8 642.44	38 22.49	22 11.88	9.57	0.3	2.41	0.09	0.2	0.2	745
910824	8 751.57	38 22.34	22 11.82	9.34	0.3	2.27	0.08	0.2	0.3	746
910824	8 8 1.87	38 22.36	22 11.88	8.97	0.3	2.40	0.09	0.2	0.3	747
910824	8 858.43	38 22.46	22 12.13	9.77	0.3	2.63	0.09	0.2	0.2	748
910824	8 52 3.96	38 22.46	22 12.00	9.81	0.3	2.56	0.10	0.2	0.2	749
910824	8 5454.95	38 22.54	22 11.92	9.88	0.4	2.50	0.09	0.2	0.3	750
910824	9 2352.77	38 22.39	22 11.81	9.99	0.4	2.50	0.08	0.3	0.5	751
910824	9 5247.12	38 14.06	22 5.08	7.50	0.6	2.54	0.13	0.3	0.3	752
910824	10 59 1.69	38 24.59	21 51.74	8.53	0.6	2.60	0.11	0.4	0.3	753
910824	11 430.96	38 21.84	22 8.27	7.45	0.2	2.37	0.05	0.1	0.2	754
910824	11 4548.86	38 23.70	21 53.85	6.96	1.1	2.36	0.13	0.4	0.4	755
910824	12 931.34	38 24.11	21 55.17	8.81	0.4	2.75	0.11	0.2	0.1	756
910824	12 36 5.88	38 22.22	22 11.79	10.07	0.2	2.67	0.09	0.2	0.3	757
910824	12 3657.79	38 22.26	22 11.34	9.78	0.2	2.03	0.03	0.2	0.3	759
910824	12 4415.98	38 21.90	22 12.18	9.58	0.5	2.39	0.10	0.4	0.5	760
910824	14 5532.25	38 22.55	22 11.86	10.09	0.4	2.82	0.15	0.3	0.2	761
910824	15 2957.97	38 21.76	22 15.33	12.36	0.2	2.46	0.03	0.5	0.4	762
910824	16 4041.85	38 21.36	22 8.39	7.13	0.3	2.29	0.10	0.3	0.4	763
910824	16 4958.94	38 22.13	22 11.58	9.54	0.4	2.19	0.07	0.4	0.5	764
910824	17 2253.09	38 22.64	22 11.81	10.76	0.4	2.67	0.12	0.4	0.3	765
910824	17 3919.63	38 22.42	22 11.81	9.52	0.3	2.21	0.05	0.3	0.3	766
910824	17 4624.73	38 22.11	22 12.58	9.21	0.4	2.30	0.06	0.4	0.4	767
910824	18 2417.30	38 22.29	22 12.04	9.87	0.5	2.35	0.08	0.5	0.5	768
910824	18 3044.95	38 22.33	22 11.95	10.10	0.4	2.39	0.08	0.4	0.5	769
910824	18 3812.37	38 22.07	22 11.94	9.83	0.3	2.19	0.06	0.2	0.2	770
910824	18 4916.92	38 23.96	22 1.05	9.23	0.2	2.44	0.02	0.1	0.2	771
910824	19 4531.78	38 22.20	22 11.91	9.74	0.3	2.21	0.08	0.4	0.4	772
910824	20 1640.56	38 30.21	21 50.88	14.11	0.3	2.30	0.04	0.2	0.3	773
910824	20 3224.69	38 14.09	22 7.92	7.76	0.7	2.59	0.15	0.5	0.4	774
910824	20 5412.38	38 22.51	22 7.95	6.28	0.4	2.40	0.07	0.2	0.4	775
910824	21 4 7.20	38 23.72	21 54.74	9.18	0.3	2.79	0.10	0.2	0.1	776
910824	21 738.14	38 22.58	22 11.60	10.46	0.3	2.35	0.06	0.5	0.5	777
910824	21 1113.41	38 22.12	22 11.45	9.95	0.3	2.36	0.04	0.2	0.3	778
910824	21 14 2.76	38 22.68	22 11.72	9.78	0.2	2.57	0.07	0.2	0.2	779
910824	21 3046.87	38 21.14	22 15.32	13.83	0.5	2.44	0.06	0.6	0.5	780
910824	22 16 2.27	38 21.57	22 4.08	10.00	0.3	2.73	0.10	0.2	0.1	781
910824	22 32 1.19	38 28.35	21 55.49	10.84	0.3	2.65	0.08	0.2	0.2	782
910824	22 36 1.84	38 22.59	22 11.83	10.07	0.2	2.70	0.09	0.2	0.2	783
910824	23 1347.80	38 36.36	21 56.34	19.89	0.5	2.38	0.08	0.2	0.5	784
910824	23 1632.33	38 34.69	21 56.02	23.05	1.5	2.39	0.05	0.5	2.4	785
910824	23 4255.69	38 36.19	21 56.47	20.99	0.5	2.39	0.08	0.2	0.6	786
910825	0 5841.55	38 22.34	22 11.74	9.70	0.3	2.41	0.07	0.2	0.3	787
910825	1 3418.75	38 14.46	22 8.00	6.69	0.7	2.51	0.19	0.6	0.4	788
910825	1 3945.99	38 13.80	22 7.70	7.74	0.6	2.51	0.13	0.4	0.3	789
910825	2 31 9.72	38 34.06	21 55.68	23.24	0.9	2.34	0.03	0.3	1.7	790

APPENDIX B (*Continued.*)

Date	Time	Lat	Long	Depth	ERZ	Mag.	RMS	ERX	ERY	n.evt
910825	4 556.74	38 20.37	21 48.56	8.32	0.5	2.82	0.11	0.3	0.1	791
910825	4 4616.40	38 10.94	22 4.89	4.50	0.5	2.46	0.13	0.2	0.2	792
910825	5 1319.02	38 22.06	22 11.71	9.60	0.4	2.41	0.08	0.3	0.3	793
910825	5 1621.73	38 22.35	22 11.84	9.67	0.4	2.84	0.13	0.3	0.2	794
910825	5 5951.93	38 25.35	22 7.96	10.96	0.2	2.36	0.05	0.1	0.3	795
910825	6 9 5.20	38 13.69	22 7.70	9.20	0.9	2.44	0.16	0.5	0.5	796
910825	6 3651.11	38 14.54	22 5.29	7.53	0.8	2.21	0.14	0.5	0.5	797
910825	6 4940.60	38 14.42	22 5.74	7.86	0.8	2.14	0.15	0.4	0.4	798
910825	7 2254.70	38 13.86	22 4.70	6.94	0.4	2.36	0.07	0.3	0.5	799
910825	7 4056.40	38 22.40	22 11.81	9.37	0.3	2.39	0.10	0.3	0.2	800
910825	9 3349.37	38 21.81	22 11.68	9.86	0.4	1.96	0.04	0.5	0.2	801
910825	9 4724.14	38 20.76	22 3.78	9.15	0.5	2.46	0.08	0.2	0.1	802
910825	11 2736.16	38 14.48	22 5.20	7.33	0.6	2.44	0.13	0.3	0.4	803
910825	11 30 2.97	38 13.86	22 5.80	7.54	0.5	2.49	0.15	0.3	0.3	804
910825	13 2029.12	38 13.62	22 5.80	7.82	0.5	2.50	0.19	0.4	0.4	805
910825	14 3555.73	38 13.76	22 3.96	6.69	0.4	2.31	0.10	0.4	0.5	806
910825	18 4 5.00	38 23.87	21 49.81	7.67	0.3	2.16	0.07	0.2	0.4	807
910825	18 2518.62	38 24.63	21 54.74	9.32	0.3	2.64	0.10	0.1	0.2	808
910825	18 4956.44	38 23.08	22 8.01	6.91	0.3	2.48	0.13	0.2	0.4	809
910825	18 5155.10	38 22.97	22 7.98	7.19	0.2	2.34	0.11	0.2	0.3	811
910825	20 1817.29	38 13.60	22 4.94	6.85	0.8	2.35	0.10	0.5	0.6	812
910825	20 3846.25	38 14.25	22 5.46	7.04	0.3	2.41	0.12	0.3	0.2	813
910825	23 10 6.98	38 24.75	22 8.13	10.99	0.5	2.39	0.04	0.5	0.4	814
910826	0 1338.87	38 34.48	21 54.47	14.30	0.5	2.35	0.10	0.2	0.4	815
910826	0 16 7.49	38 22.14	21 53.48	6.68	0.7	2.24	0.09	0.3	0.3	816
910826	1 3214.75	38 24.74	21 58.40	8.79	1.9	2.27	0.12	1.7	0.5	817
910826	1 4317.41	38 24.27	21 57.77	7.13	0.4	1.94	0.09	0.2	0.2	818

Date	Time	Lat	Long	Depth	ERZ	Mag.	RMS	ERX	ERY	n.evt
910826	1 4317.41	38 24.27	21 57.77	7.13	0.4	1.94	0.09	0.2	0.2	818
910826	1 5632.37	38 13.94	22 5.91	7.89	0.4	2.59	0.16	0.3	0.2	819
910826	2 743.46	38 25.24	22 8.27	10.61	0.9	2.25	0.11	0.6	0.8	820
910826	2 33 2.76	38 22.69	22 8.31	6.57	0.6	2.25	0.09	0.2	0.3	821
910826	3 813.45	38 16.14	22 3.73	11.97	2.3	0.00	0.14	0.7	0.5	822
910826	4 149.52	38 14.11	22 5.46	8.00	0.4	2.53	0.16	0.3	0.2	823
910826	4 1423.63	38 22.65	22 0.01	7.88	0.4	1.86	0.05	0.2	0.2	824
910826	4 1434.31	38 23.09	22 0.35	8.62	0.5	2.06	0.11	0.3	0.3	825
910826	6 2140.32	38 18.49	21 52.98	7.80	0.5	2.75	0.11	0.3	0.2	826
910826	8 1826.91	38 28.99	21 58.59	12.28	0.4	2.49	0.11	0.3	0.3	827
910826	8 3755.60	38 18.35	22 18.99	10.46	0.9	2.76	0.11	0.7	0.4	828
910826	9 13 2.50	38 13.87	22 6.05	7.37	0.5	2.55	0.16	0.3	0.3	829
910826	9 2911.82	38 20.50	22 5.95	8.00	0.3	2.14	0.08	0.2	0.2	830
910826	10 841.93	38 23.56	21 49.69	9.32	2.0	2.67	0.12	1.0	0.5	831
910826	11 3417.67	38 21.68	22 1.03	9.51	0.3	2.62	0.07	0.2	0.1	833
910826	16 1259.39	38 19.02	21 59.21	7.15	0.2	2.59	0.11	0.3	0.1	834
910826	18 5614.29	38 24.96	21 55.12	10.18	0.4	2.50	0.04	0.4	0.3	835
910826	19 1450.34	38 14.17	22 5.52	5.98	0.9	2.35	0.14	0.6	0.4	836
910826	20 3311.15	38 24.61	21 58.94	8.55	0.4	2.44	0.08	0.3	0.3	837
910826	22 3928.52	38 22.08	22 0.40	6.79	0.7	2.46	0.12	0.4	0.3	838
910827	3 1510.05	38 14.61	22 5.10	7.53	0.5	2.42	0.14	0.2	0.2	842
910827	3 5411.37	38 24.32	21 55.82	8.59	0.8	2.68	0.12	0.4	0.3	843
910827	4 828.08	38 18.02	22 9.02	6.10	0.5	2.46	0.08	0.3	0.1	844
910827	4 5822.36	38 22.86	22 8.53	7.02	0.8	2.87	0.20	0.6	0.7	845
910827	5 4953.42	38 23.91	21 49.22	9.85	1.7	2.81	0.05	0.9	0.6	846
910827	8 2640.22	38 14.67	22 5.89	8.40	0.8	2.46	0.09	0.3	0.3	847
910827	8 5250.32	38 18.83	22 4.72	8.98	0.8	2.65	0.09	0.5	0.2	848

APPENDIX C: FOCAL MECHANISMS

Lower hemisphere ●: compression - ○: dilatation - Smallest same dots for refracted rays

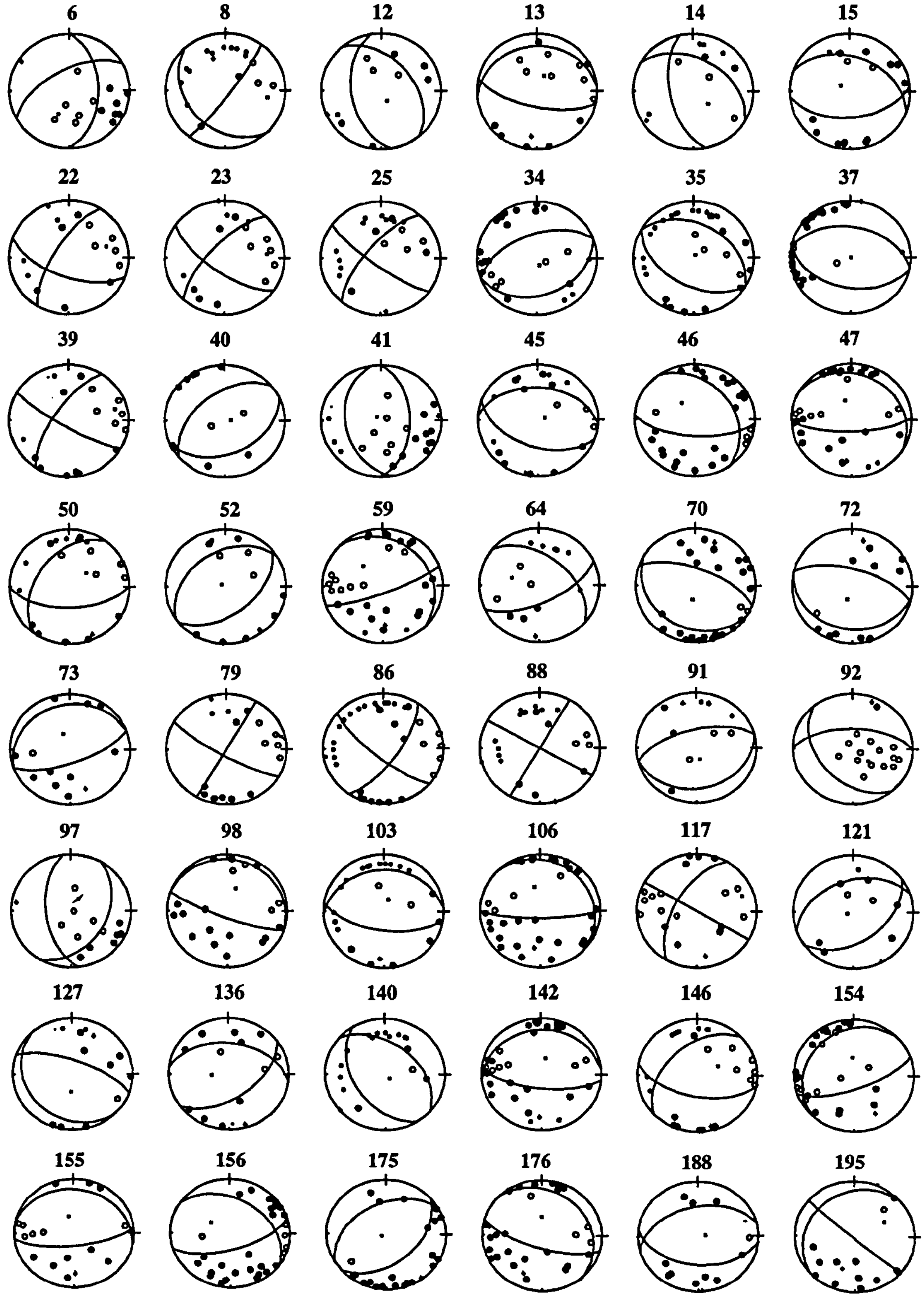

APPENDIX C (*Continued.*)

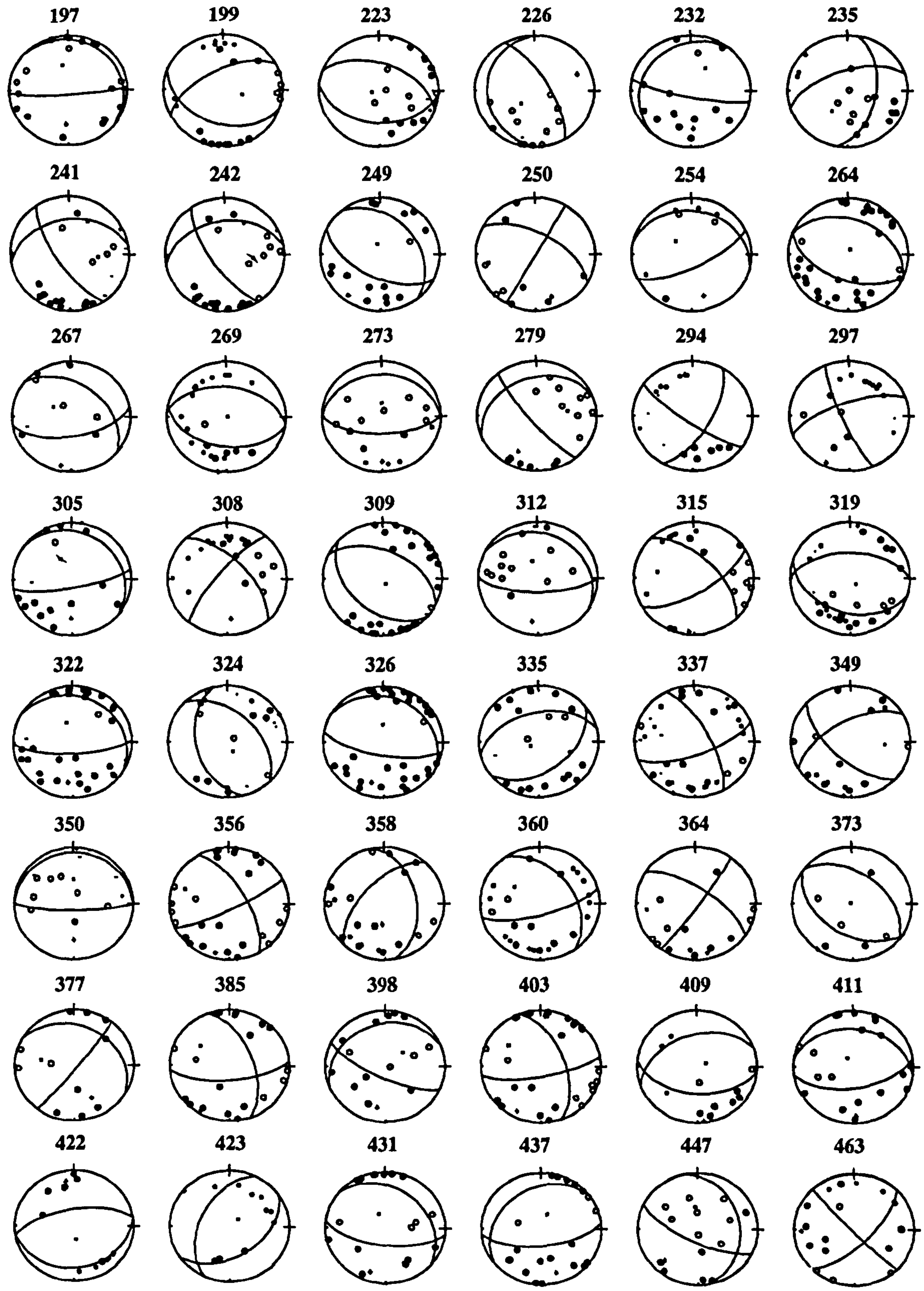

APPENDIX C (*Continued.*)

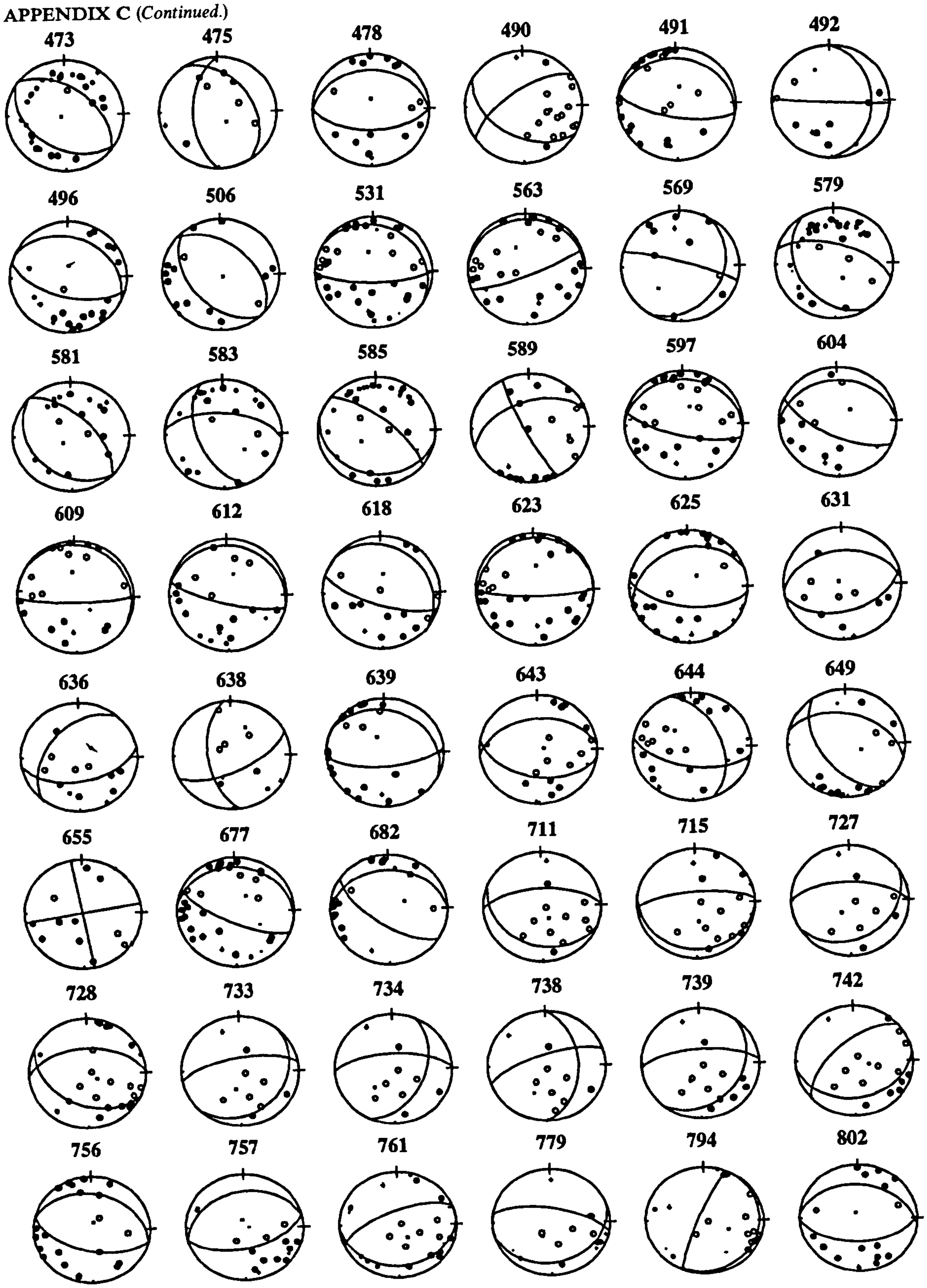

APPENDIX C (*Continued.*)

809 **811** **819** **843**

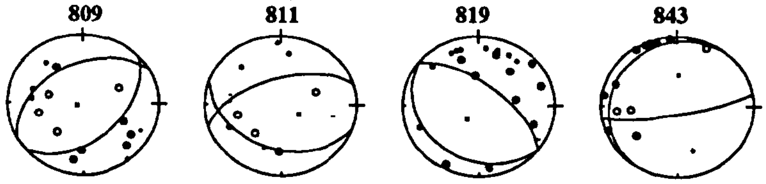

APPENDIX D: FOCAL MECHANISM PARAMETERS

Event	Str1	Dip1	Slip1	Str2	Dip2	Slip2
6	0.0	50.0	-139.9	241.6	60.5	-47.6
8	37.0	83.0	124.7	137.0	35.3	12.2
12	320.0	45.0	-112.2	170.0	49.1	-69.3
13	265.0	23.0	-105.7	102.0	67.9	-83.4
14	300.0	43.0	-129.1	168.0	58.0	-59.5
15	290.0	40.0	-70.0	84.6	52.8	-106.0
22	211.0	70.0	-150.4	110.0	62.3	-22.7
23	223.0	70.0	-157.7	125.0	69.1	-21.5
25	220.0	70.0	-168.4	126.0	79.2	-20.4
34	69.0	35.0	-90.0	249.0	55.0	-90.0
35	120.0	50.0	-90.0	300.0	40.0	-90.0
37	102.0	45.0	-88.6	280.0	45.0	-91.4
39	120.0	80.0	-19.9	213.6	70.4	-169.4
40	230.0	50.0	-99.8	65.0	41.0	-78.6
41	170.0	40.0	-97.9	0.3	50.5	-83.4
45	110.0	50.0	-79.6	274.0	41.1	-102.2
46	324.0	35.0	-45.7	94.0	65.8	-116.1
47	300.0	20.0	-59.6	88.0	72.8	-100.4
50	89.0	60.0	-56.4	216.0	43.8	-133.8
52	51.0	51.0	-93.2	236.0	39.1	-86.1
59	70.0	80.0	-110.0	314.5	22.3	-27.3
64	310.0	48.0	-34.9	65.0	64.9	-132.3
70	290.0	65.0	-94.3	120.0	25.3	-80.9
72	285.0	65.0	-87.9	100.0	25.1	-94.5
73	70.0	70.0	-90.0	250.0	20.0	-90.0
79	120.0	80.0	180.0	210.0	90.0	0.0
86	35.0	70.0	165.7	130.0	76.5	20.6
88	210.0	90.0	0.0	300.0	90.0	180.0
91	75.0	27.0	-90.0	255.0	63.0	-90.0
92	270.0	60.0	-120.0	139.1	41.4	-49.1
97	30.0	40.0	-60.0	173.0	56.2	-112.8
98	110.0	80.0	-90.0	290.0	10.0	-90.0
103	267.0	28.0	-99.7	98.0	62.4	-84.9
106	90.0	80.0	-100.0	315.4	14.1	-45.5
117	210.0	60.0	0.0	300.0	90.0	180.0
121	250.0	44.0	-78.3	54.0	47.1	-101.0
127	290.0	70.0	-100.0	137.3	22.3	-64.5
136	277.0	44.0	-56.1	54.0	54.8	-118.3
140	311.0	45.0	-102.2	148.0	46.3	-78.1
142	96.0	69.0	-85.6	264.0	21.4	-101.2
146	101.0	59.0	-53.7	226.0	46.3	-134.6
154	70.0	70.0	-80.1	223.0	22.2	-115.3
155	84.0	71.0	-96.0	282.0	19.9	-73.0
156	73.0	65.0	-118.4	305.0	37.1	-44.4
175	48.0	47.0	-98.2	240.0	43.6	-81.3
176	106.0	71.0	-100.6	316.0	21.7	-61.8

APPENDIX D (*Continued.*)

Event	Str1	Dip1	Slip1	Str2	Dip2	Slip2
188	256.0	45.0	-104.4	96.0	46.8	-76.0
195	130.0	87.0	-66.9	227.0	23.3	-172.4
197	311.0	11.0	-46.5	87.0	82.0	-97.6
199	110.0	39.0	-49.2	242.0	61.5	-117.9
223	290.0	50.0	-79.6	94.0	41.1	-102.2
226	330.0	70.0	-100.0	177.3	22.3	-64.5
232	220.0	20.0	-150.0	101.5	80.1	-72.5
235	10.0	50.0	-140.0	251.7	60.5	-47.6
241	260.0	40.0	-149.8	146.0	71.2	-54.0
242	260.0	40.0	-150.0	146.1	71.2	-54.0
249	321.0	36.0	-70.2	117.0	56.4	-103.8
250	30.0	89.0	-149.0	299.4	59.0	-1.2
254	282.0	23.0	-54.3	64.0	71.5	-103.9
264	112.0	53.0	-90.0	292.0	37.0	-90.0
267	80.0	60.0	-120.0	309.1	41.4	-49.1
269	276.0	45.0	-92.8	100.0	45.1	-87.2
273	90.0	65.0	-90.0	270.0	25.0	-90.0
279	140.0	80.0	-59.9	246.7	31.5	-160.6
294	30.0	65.0	168.3	125.0	79.4	25.5
297	250.0	70.0	-169.9	156.5	80.5	-20.3
305	80.0	77.0	-104.0	308.0	19.0	-43.6
308	317.0	62.0	14.7	220.0	77.1	151.2
309	296.0	49.0	-100.7	132.0	42.1	-78.0
312	90.0	70.0	-100.0	297.3	22.3	-64.5
315	59.0	68.0	-146.4	315.0	59.1	-25.9
319	108.0	39.0	-75.8	270.0	52.4	-101.2
322	300.0	20.0	-60.0	88.4	72.8	-100.3
324	315.0	48.0	-111.9	166.0	46.4	-67.5
326	300.0	21.0	-71.2	100.0	70.2	-97.0
335	256.0	47.0	-73.1	52.0	45.6	-107.3
337	332.0	69.0	-21.4	70.0	70.1	-157.6
349	240.0	60.0	-148.6	133.0	63.1	-34.1
350	90.0	80.0	-90.0	270.0	10.0	-90.0
356	330.0	66.0	-9.8	64.0	81.1	-155.7
358	350.0	45.0	46.8	223.0	59.0	124.4
360	75.0	73.0	-128.8	325.0	41.8	-26.0
364	36.0	85.0	-158.2	304.0	68.3	-5.4
373	308.0	45.0	-87.2	124.0	45.1	-92.8
377	300.0	30.0	-10.0	38.7	85.0	-119.6
385	85.0	68.0	-144.4	340.0	57.4	-26.4
398	115.0	73.0	-72.0	247.0	24.6	-135.3
403	80.0	75.0	-145.7	340.0	57.1	-18.0
409	95.0	50.0	-73.3	250.0	42.8	-108.9
411	81.0	59.0	-98.9	278.0	32.1	-75.5
422	80.0	25.0	-90.0	260.0	65.0	-90.0
423	55.0	45.0	-67.8	205.0	49.1	-110.7
431	310.0	30.0	-60.0	96.3	64.3	-106.1
437	84.0	65.0	-75.2	232.0	28.8	-118.7
447	350.0	30.0	-40.0	116.0	71.3	-113.9
463	45.0	68.0	-2.7	136.0	87.5	-158.0
473	124.0	40.0	-93.8	309.0	50.1	-86.8
475	180.0	55.0	-69.6	327.0	39.9	-116.5
478	90.0	60.0	-90.0	270.0	30.0	-90.0
490	120.0	45.0	-34.6	236.0	66.3	-129.5
491	100.0	70.0	-90.0	280.0	20.0	-90.0
496	295.0	30.0	-81.3	105.0	60.4	-95.0
506	312.0	45.0	-95.7	140.0	45.3	-84.4
531	90.0	75.0	-99.2	302.0	17.5	-59.2
563	270.0	10.0	-70.0	69.7	80.6	-93.5
569	286.0	83.0	-62.2	29.0	28.6	-165.3
579	286.0	61.0	-113.6	148.0	36.7	-54.2
581	316.0	59.0	-89.0	134.0	31.0	-91.7
583	275.0	58.0	-136.1	158.0	54.0	-40.9
585	310.0	70.0	-80.1	103.0	22.2	-115.3
589	250.0	50.0	-169.9	153.5	82.3	-40.4
597	274.0	17.0	-99.6	104.0	73.2	-87.1
604	268.0	25.0	-115.7	116.0	67.6	-78.6
609	300.0	9.0	-60.3	90.0	82.2	-94.5
612	281.0	13.0	-92.9	104.0	77.0	-89.3
618	310.0	20.0	-69.2	108.0	71.4	-97.4
623	250.0	10.0	-110.0	90.3	80.6	-86.5
625	97.0	61.0	-76.7	251.0	31.7	-112.5
631	264.0	41.0	-83.9	76.0	49.3	-95.2
636	80.0	53.0	-63.2	220.0	44.5	-120.9
638	65.0	65.0	-37.6	173.0	56.5	-149.5
639	86.0	69.0	-101.7	296.0	23.9	-62.2
643	265.0	43.0	-101.1	100.0	48.0	-79.8
644	100.0	60.0	-130.0	339.2	48.4	-41.9
649	285.0	45.0	-121.6	146.0	53.0	-62.4
655	80.0	90.0	180.0	170.0	90.0	0.0
677	276.0	19.0	-107.1	114.0	71.9	-84.2
682	269.0	29.0	-121.5	124.0	65.6	-73.9
711	112.0	29.0	-68.7	268.0	63.1	-101.4
715	94.0	17.0	-82.3	266.0	73.2	-92.3
727	58.0	31.0	-118.2	270.0	63.0	-74.2
728	116.0	41.0	-68.1	268.0	52.5	-107.9
733	42.0	25.0	-125.3	260.0	69.8	-74.9
734	24.0	45.0	-145.4	268.0	66.3	-50.5
738	0.0	45.0	-155.3	252.0	72.8	-47.7
739	38.0	31.0	-133.6	266.0	68.1	-67.5
742	80.0	33.0	-63.3	229.0	60.9	-106.3
756	284.0	33.0	-90.0	104.0	57.0	-90.0
757	76.0	57.0	-90.0	256.0	33.0	-90.0
761	85.0	23.0	-74.3	248.0	67.9	-96.6
779	72.0	25.0	-115.7	280.0	67.6	-78.6
794	28.0	9.0	-85.1	203.0	81.0	-90.8
802	276.0	37.0	-83.6	88.0	53.3	-94.8
809	47.0	47.0	-98.9	240.0	43.7	-80.5
811	110.0	37.0	-58.0	252.0	59.3	-111.7
819	308.0	65.0	-90.0	128.0	25.0	-90.0
843	80.0	80.0	-80.1	215.0	14.0	-134.1